

Impact of different extended components of mean field models on transport coefficients of quark matter and their causal aspects

Chowdhury Aminul Islam*

Department of theoretical Physics, Tata Institute of fundamental Research, Homi Bhabha Road, Mumbai 400005, India

Jayanta Dey[†] and Sabyasachi Ghosh[‡]

Indian Institute of Technology Bhilai, GEC Campus, Sejbahar, Raipur 492015, Chhattisgarh, India

Role of different extensions of Nambu–Jona-Lasinio (NJL) model like addition of vector interaction, Polyakov loop extended version (PNJL) and the entangled PNJL (EPNJL) models on transport coefficients like shear viscosity, bulk viscosity, electrical conductivity and thermal conductivity are critically analyzed. We have considered the standard expressions of transport coefficients, obtained in relaxation time approximation of kinetic theory. Influence of temperature dependent order parameters on temperature profile of transport coefficients are analyzed. Causal aspect of massless case to these different extended components of mean field models are also picturized, where an approximated lower and upper bound are drawn for shear relaxation time.

PACS numbers:

I. INTRODUCTION

Microscopic calculations of transport coefficients for highly dense quark matter, which may be seen in astrophysical object like compact stars, are an important input in modeling an array of astrophysical phenomena. Refs. [1–4] have gone through these microscopic estimations. Future experimental facilities, such as Facility for Antiproton and Ion Research at GSI, Germany [5] and the NICA at JINR, Russia [6] aim to probe similar kind of high density zone in their laboratories. Transport coefficients of highly dense matter, produced there, may have influence on different phenomenological quantities like spectra, flow, which can be constructed from experimental data, measured by their detector set up.

On the other hand, a baryon free hot system can also be a matter of interest to know its transport coefficients values. It is believed that our early universe went through this state, just after few micro second from big-bang. RHIC experiments at BNL, USA and LHC experiments at CERN, Switzerland had reached this high temperature and baryon free zone and their experimental data [7–12] indicate that the matter almost behave like a nearly perfect fluid. A very small values of shear viscosity to entropy density ratio η/s corresponds to this nature and this small values of η/s has been searched as input guess values in viscous hydrodynamic model analysis during the matching experimental data of elliptic flow [13–15]. This small value of η/s from experimental side throws a challenge to the theoretical side, where microscopic calculations of η/s for quark matter

can be done. Estimated values of η/s from perturbative quantum chromodynamics (pQCD) at leading order [16, 17] are found to be quite larger than its experimental value. However, Ref. [18] has recently found a significant drop of this value in next-to-leading order calculation but at the end of the article, the possibility of non-perturbative components in η/s has not been ruled out. The non-perturbative temperature domain of QCD can be well mimicked by effective QCD model calculations like Nambu–Jona-Lasinio (NJL) model and quark-meson (QM) models. In Refs [19–31], this type microscopic calculation of shear viscosity via different effective QCD models has been performed. Among them, Refs. [19–28] have adopted NJL model, Ref. [31] has further incorporated the background gauge field through its Polyakov extended version. There are many possible additional sources by which NJL model can be modified into different versions. For example, addition of vector interaction, Polyakov loop extension, entangled Polyakov loop extensions can modify the NJL model structure. In present article, we have tried to investigate the impact of the different additional sources of NJL model on η/s calculations as well as for other transport coefficients like bulk viscosity, electrical conductivity and thermal conductivity.

The article is organized as follows. In Sec. II, formalism part of different versions of NJL model has been briefly addressed and in Sec. III, the expressions of different transport coefficients are derived in kinetic theory framework along with their causal extensions. Then, Sec. IV has provided the detail numerical discussion, which have explored the impact of different extensions of NJL model on transport coefficient and at last, we have summarized our studies.

*Electronic address: chowdhury.aminulislam@gmail.com

[†]Electronic address: jayantad@iitbhlai.ac.in

[‡]Electronic address: sabyaphy@gmail.com

II. FORMALISM OF NJL MODEL WITH DIFFERENT EXTENSIONS

In this section we briefly discuss the mean field models that we have employed in our work. First we talk about the NJL model for two flavor case and introduce vector interaction in the picture. Then we extend it by introducing the Polyakov loop field known as PNJL model, through which the deconfinement dynamics can be mimicked. In PNJL model the correlation between the chiral and deconfinement dynamics is weak. We impose a strong correlation between these two through Polyakov loop dependent coupling constants – this is known as entangled PNJL (EPNJL) model.

A. NJL

Let us start with NJL model first. Here we are interested in two light quark flavors and we also include the isoscalar vector interaction which plays crucial role specially for system with finite density. The Lagrangian is [32–35]:

$$\mathcal{L}_{\text{NJL}} = \bar{\psi}(i\gamma_\mu\partial^\mu - m_0 + \gamma_0\mu)\psi + \frac{G_S}{2}[(\bar{\psi}\psi)^2 + (\bar{\psi}i\gamma_5\vec{\tau}\psi)^2] - \frac{G_V}{2}(\bar{\psi}\gamma_\mu\psi)^2, \quad (1)$$

where, $m_0 = m_0 \times \mathbf{1}$, with $\mathbf{1}$ being the identity matrix and $m_u = m_d = m_0$; μ is the chemical potential; $\vec{\tau}$ is Pauli matrix; G_S and G_V are the four scalar and isoscalar-vector type coupling constants, respectively. The value of G_V is not fixed through parameter fitting, rather it is used as a free parameter which can take values within the range $0 \leq G_V/G_S \leq 1$. With the inclusion of vector interaction we now have another condensate as quark number density $n = \langle \bar{\psi}\gamma^0\psi \rangle$ [35, 36] along with the usual chiral condensate $\Sigma = \langle \bar{\psi}\psi \rangle$. Chiral condensate will build the link between current quark mass m_0 and constituent quark mass M via the relation

$$M = m_0 + 2G_S N_c N_f \int \frac{d^3\mathbf{p}}{(2\pi)^3} \frac{M}{E} (1 - f_Q - f_{\bar{Q}}), \quad (2)$$

where

$$f_{Q,\bar{Q}} = \frac{1}{e^{(E \mp \tilde{\mu})/T} + 1}, \quad (3)$$

and quark number density make the quark chemical potential μ shift to an effective chemical potential

$$\tilde{\mu} = \mu - G_V n. \quad (4)$$

Since, NJL is not renormalizable, we regularize the diverging vacuum integral by introducing a sharp three momentum cut-off Λ . The energy of the quasi-quark (both up and down) of constituent mass M is given as $E = \sqrt{\mathbf{p}^2 + M^2}$. The chiral condensate Σ at finite

temperature depends on Fermi-Dirac distribution function, which is the function of effective chemical potential, given in Eq. (4). Hence, G_V dependence enters to the Gap equation through this thermodynamical phase space. This gap Eq. (2) is plotted in Fig. (1) for different values of G_V and we find a mild noticeable enhancement of M with G_V in the intermediate temperature range. Decreasing of quark chemical potential with G_V make thermal part shrink. Therefore, the contribution of [vacuum - thermal]-term in the left hand side of (self-consistent) Eq. (2) is increased, for which we are getting a increasing trend of M with G_V . We can get back to the usual NJL Lagrangian by switching the vector interaction off.

With all these in hand, we can now write the thermodynamic potential using mean field approximation as

$$\begin{aligned} \Omega_{\text{NJL}} = & \frac{G_S}{2}\Sigma^2 - \frac{G_V}{2}n^2 - 2N_f N_c \int_\Lambda \frac{d^3\mathbf{p}}{(2\pi)^3} E \\ & - 2N_f N_c T \int \frac{d^3\mathbf{p}}{(2\pi)^3} \left[\ln(1 + e^{-(E-\tilde{\mu})/T}) \right. \\ & \left. + \ln(1 + e^{-(E+\tilde{\mu})/T}) \right]. \end{aligned} \quad (5)$$

The thermodynamic potential depends on both constituent quark mass (M) and the effective chemical potential ($\tilde{\mu}$).

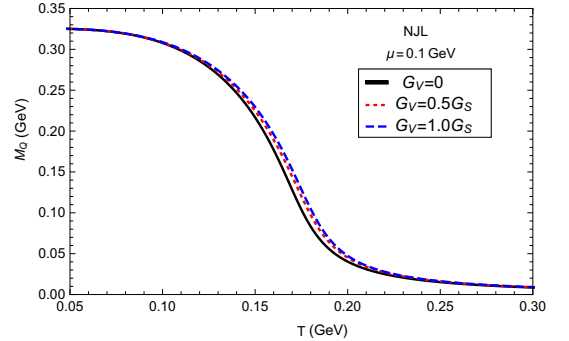


FIG. 1: Temperature dependence of constituent quark masses for $\frac{G_V}{G_S} = 0$ (solid line), 0.5 (dotted line), 1 (dashed line) at $\mu = 0.1$ GeV.

B. PNJL

So far we have considered only the chiral dynamics, by which quark to hadron phase transition can be realized as restored to broken phases of chiral symmetry. Now we also incorporate the deconfinement dynamics by including Polyakov loop. It will give us another view, where we can see the quark to hadron phase transition as a confinement to deconfinement phase transition. This is formally known as PNJL model [37–42]. Here along with the Σ and n fields we have two more mean fields – expectation value of Polyakov loop Φ and its conjugate $\bar{\Phi}$. Φ works

as the order parameter for deconfinement dynamics. For two flavor the PNJL Lagrangian with vector interaction is written as

$$\begin{aligned}\mathcal{L}_{\text{PNJL}} = & \bar{\psi}(i\mathcal{D} - m_0 + \gamma_0\mu)\psi + \frac{G_S}{2}[(\bar{\psi}\psi)^2 \\ & + (\bar{\psi}i\gamma_5\vec{\tau}\psi)^2] - \frac{G_V}{2}(\bar{\psi}\gamma_\mu\psi)^2 \\ & - \mathcal{U}(\Phi[A], \bar{\Phi}[A], T),\end{aligned}\quad (6)$$

where where $\mathcal{D} = \gamma_\mu D^\mu$ and the covariant derivative $D^\mu = \partial^\mu - ig\mathcal{A}_a^\mu\lambda_a/2$, $\mathcal{A}_a^\mu = \delta^{\mu 0}\mathcal{A}_0^a$ being the $SU(3)$ background fields; λ_a 's are the Gell-Mann matrices. One should note that here only two components of the gauge field, corresponding to λ_3 and λ_8 , will contribute. The effective Polyakov loop gauge potential is parameterized as

$$\frac{\mathcal{U}(\Phi, \bar{\Phi}, T)}{T^4} = -\frac{b_2(T)}{2}\Phi\bar{\Phi} - \frac{b_3}{6}(\Phi^3 + \bar{\Phi}^3) + \frac{b_4}{4}(\Phi\bar{\Phi})^2, \quad (7)$$

with

$$b_2(T) = a_0 + a_1\left(\frac{T_0}{T}\right) + a_2\left(\frac{T_0}{T}\right)^2 + a_3\left(\frac{T_0}{T}\right)^3. \quad (8)$$

Values of different coefficients and parameters $a_0, a_1, a_2, a_3, b_3, b_4, T_0$ and κ are same as those given in Refs. [40, 43]. We should note an important point here

that in the NJL model the color trace gives us a factor of N_c . In the presence of background gauge field the color trace is not straightforward. After some mathematical manipulation the color trace in PNJL model also splits out a factor of N_c along with a modified thermal distribution function for particle and antiparticle which read as [43, 44]

$$\begin{aligned}f_Q &= \frac{\Phi e^{-\beta(E-\tilde{\mu})} + 2\bar{\Phi}e^{-2\beta(E-\tilde{\mu})} + e^{-3\beta(E-\tilde{\mu})}}{1 + 3\Phi e^{-\beta(E-\tilde{\mu})} + 3\bar{\Phi}e^{-2\beta(E-\tilde{\mu})} + e^{-3\beta(E-\tilde{\mu})}}, \\ f_{\bar{Q}} &= \frac{\bar{\Phi}e^{-\beta(E+\tilde{\mu})} + 2\Phi e^{-2\beta(E+\tilde{\mu})} + e^{-3\beta(E+\tilde{\mu})}}{1 + 3\bar{\Phi}e^{-\beta(E+\tilde{\mu})} + 3\Phi e^{-2\beta(E+\tilde{\mu})} + e^{-3\beta(E+\tilde{\mu})}}\end{aligned}\quad (9)$$

respectively. We get back the usual NJL results from these distribution functions by putting $\Phi = \bar{\Phi} = 1$. Thus while calculating different transport coefficients in the ambient of these models one needs to be careful. For NJL model it will be sufficient to replace the usual mass by the effective one. But for PNJL model one also needs to incorporate the modified distribution functions (See Refs. [30]). With these modified distribution functions the effective mass in PNJL model reads as

$$M = m_0 + 2G_S N_c N_f \int \frac{d^3\mathbf{p}}{(2\pi)^3} \frac{M}{E} (1 - f_Q - f_{\bar{Q}}). \quad (10)$$

The corresponding thermodynamic potential is written as

$$\begin{aligned}\Omega_{\text{PNJL}} = & \mathcal{U}(\Phi, \bar{\Phi}, T) + \frac{G_S}{2}\Sigma^2 - \frac{G_V}{2}n^2 \\ & - 2N_f T \int \frac{d^3\mathbf{p}}{(2\pi)^3} \ln \left[1 + 3 \left(\Phi + \bar{\Phi}e^{-(E-\tilde{\mu})/T} \right) e^{-(E-\tilde{\mu})/T} + e^{-3(E-\tilde{\mu})/T} \right] \\ & - 2N_f T \int \frac{d^3\mathbf{p}}{(2\pi)^3} \ln \left[1 + 3 \left(\bar{\Phi} + \Phi e^{-(E+\tilde{\mu})/T} \right) e^{-(E+\tilde{\mu})/T} + e^{-3(E+\tilde{\mu})/T} \right] \\ & - \kappa T^4 \ln[J(\Phi, \bar{\Phi})] - 2N_f N_c \int_\Lambda \frac{d^3\mathbf{p}}{(2\pi)^3} E.\end{aligned}\quad (11)$$

The Vandermonde determinant $J(\Phi, \bar{\Phi})$ is given by [40, 45]

$$J[\Phi, \bar{\Phi}] = \frac{27}{24\pi^2} \left[1 - 6\Phi\bar{\Phi} + 4(\Phi^3 + \bar{\Phi}^3) - 3(\Phi\bar{\Phi})^2 \right]. \quad (12)$$

C. EPNJL

It has been confirmed through different lattice QCD simulation that chiral and deconfinement transitions take place at the same temperature [46] or nearly the same temperature [47]. Now this is not clearly understood whether it is a mere coincidence or there are some cor-

relations between these two apparently distinct phenomena. To understand this coincidence through effective models a conjecture of strong entanglement between the chiral and deconfinement dynamics has been proposed [48, 49]. Because of this entanglement of two dynamics it is known as EPNJL model. This is realized by introducing Polyakov loop dependent coupling constants, where the form of the ansatz is so chosen that it is Z_3 symmetric. Thus the Lagrangian in EPNJL model is same as that in (6) except the coupling constants G_S and G_V are now replaced by $\tilde{G}_S(\Phi)$ and $\tilde{G}_V(\Phi)$. They are given by

$$\tilde{G}_S(\Phi) = G_S[1 - \alpha_1\Phi\bar{\Phi} - \alpha_2(\Phi^3 + \bar{\Phi}^3)], \quad (13)$$

and

$$\tilde{G}_V(\Phi) = G_V[1 - \alpha_1\Phi\bar{\Phi} - \alpha_2(\Phi^3 + \bar{\Phi}^3)]. \quad (14)$$

If we put $\alpha_1 = \alpha_2 = 0$ we get back usual PNJL model. The strength of the vector coupling constant is, as mentioned earlier, taken in terms of values of G_S . In the same way we can get the thermodynamic potential for EPNJL model by introducing Polyakov loop dependent coupling constants in Eq. (11). Now along with all the parameters

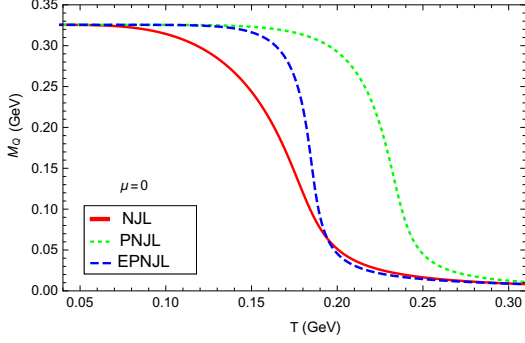


FIG. 2: Temperature dependence of constituent quark masses for NJL (solid line), PNJL (dotted line), EPNJL (dashed line) at $\mu = 0$.

in PNJL model we have two new parameters, α_1 and α_2 which need to be fixed. This is done and discussed in details in [50]. It is found there that the values of $(\alpha_1, \alpha_2) = (0.1, 0.1)$ allow to reproduce the coincidence of two transition temperatures to be within the range provided by lattice QCD for zero chemical potential [51, 52]. The explicit form of the gap equation in EPNJL model is the same as that written in Eq. (10) except that G_S and G_V will now be replaced by \tilde{G}_S and \tilde{G}_V as given in Eqs. (13) and (14) respectively.

The picture of transition from a current quark mass $m_0 \approx 0.010$ GeV at high T to constituent quark mass $M \approx 0.320$ GeV at low T will mainly map the quark-hadron phase transition and maximum transition of mass is occurred at transition temperature point. In different extended NJL models, this point is shifted. Fig. (2) demonstrates it nicely.

Let us start with the discussion of transition temperature for NJL model first. From the melting of $M(T)$ curve (red solid line) for NJL model, one can recognize roughly the maximum melting point as $T_\Sigma \approx 0.177$ GeV (at $\mu = 0$). It is only chiral dynamics which is associated with this mass melting in NJL model, therefore, T_Σ is popularly known as chiral transition temperature. As we increase μ the transition temperature keeps on decreasing. On the other hand in PNJL model we have both chiral and deconfinement dynamics. So essentially we have two phase transitions – one is the chiral phase transition, occurred at T_Σ and the other is the deconfinement phase transition, occurred at temperature T_Φ (say). In PNJL model, at $\mu = 0$, we have found $T_\Sigma = 0.233$ GeV and

$T_\Phi = 0.228$ GeV (for $\mu = 0$, $\Phi = \bar{\Phi}$, so we have $T_\Phi = T_{\bar{\Phi}}$) by searching the inflection points of quark condensate and Polyakov loop, respectively[72]. As we increase μ both transition temperatures decrease and also there is now differences between T_Φ and $T_{\bar{\Phi}}$ for nonzero μ , though very small. We take average of the two temperatures $(\frac{T_\Phi + T_{\bar{\Phi}}}{2})$ to denote the deconfinement temperatures for nonzero values of μ . Since the chiral transition temperature is always very close to the deconfinement transition temperature, we use the average of the two $(\frac{T_\Sigma + T_\Phi}{2})$ to denote as the critical temperature in PNJL model. In EPNJL model with the parameter choice $(\alpha_1, \alpha_2) = (0.1, 0.1)$ we get $T_\Sigma = 185$ MeV and $T_\Phi = 183$ MeV at $\mu = 0$ [50].

D. Thermodynamical quantities

We see that the thermal distributions, denoted by $f_{Q,\bar{Q}}$, are taking different forms in different versions of the model. In NJL model it is the usual FD distribution function with the effective mass (M_Q) and chemical potential ($\tilde{\mu}$), as given in Eq. (3). In absence of vector interaction, $\tilde{\mu}$ reduces to μ . When we deal with PNJL model the FD distributions transform to some modified forms, as given in Eq. (9). Apart from these palpable differences in forms, distributions in NJL and PNJL models are also different through the constituent quark masses, which are different for these two models (vide Fig. 2). The form of the distributions remain the same in PNJL and EPNJL models, but quantitatively they are again different because of their differences in effective mass (Fig. 2).

Now, in general, if we denote $f_{Q\bar{Q}}$ as thermal distribution functions, then we can present our different thermodynamical quantities in terms of $f_{Q\bar{Q}}$, owing to the quasi-particle relation of statistical mechanics. Thermodynamical quantities like pressure P , the energy density ϵ , and net quark or baryon density ρ can be obtained from the quasi-particle relations [27]

$$P = 2N_f N_c \int \frac{d^3\mathbf{p}}{(2\pi)^3} \frac{\mathbf{p}^2}{3E} [f_Q + f_{\bar{Q}}], \quad (15)$$

$$\epsilon = 2N_f N_c \int \frac{d^3\mathbf{p}}{(2\pi)^3} E [f_Q + f_{\bar{Q}}], \quad (16)$$

$$\rho = 2N_f N_c \int \frac{d^3\mathbf{p}}{(2\pi)^3} [f_Q - f_{\bar{Q}}]. \quad (17)$$

The entropy density s and the heat function h are related to the above quantities through the following relations:

$$s = \frac{\epsilon + P - \mu\rho}{T}, \quad (18)$$

$$h = (\epsilon + P)/\rho. \quad (19)$$

Heat function h is an important quantity, defined by the ratio of enthalpy density ($\epsilon + P$) to the net quark density (ρ). This quantity becomes divergent (unphysical) at $\mu =$

0, where net quark density vanishes. However, enthalpy density $h\rho = \epsilon + P$ remain finite.

III. TRANSPORT COEFFICIENTS

A detail derivation of the expressions of transport coefficients from relaxation time approximation (RTA) can be seen in Refs. [28, 54–56, 66, 67], and from Kubo approach in Refs. [57–59]. In this section, we will take a revisit of RTA methodology just for a sequential description.

To calculate different transport coefficients of relativistic fluid, the necessary macroscopic quantities are energy-momentum tensor ($T^{\mu\nu}$), four dimensional quark/baryon current (N^μ) and electric current (J^μ). Here, 4-vectors are represents by Greek letters and 3-vectors are represents by Latin letters. If we consider that the fluid is made up of 2-flavor quark and anti-quark, then in microscopic kinetic theory the macroscopic quantities can be expressed as

$$T^{\mu\nu} = 2N_f N_c \int \frac{d^3\mathbf{p}}{(2\pi)^3} \frac{p^\mu p^\nu}{E} (f_Q + f_{\bar{Q}}), \quad (20)$$

$$N^\mu = 2N_f N_c \int \frac{d^3\mathbf{p}}{(2\pi)^3} \frac{p^\mu}{E} (f_Q - f_{\bar{Q}}) \text{ and} \quad (21)$$

$$J^\mu = 2N_c \sum_{u,d} \int \frac{d^3\mathbf{p}}{(2\pi)^3} \frac{p^\mu}{E} (e_Q f_Q + e_{\bar{Q}} f_{\bar{Q}}), \quad (22)$$

where flavor degeneracy $N_f = 2$; color degeneracy $N_c = 3$; the summation stands for 2 flavor quark and anti-quark to account for their charges ($e_{u,\bar{u}} = \pm 2e/3$ and $e_{d,\bar{d}} = \mp e/3$); particle four momentum $p^\mu = (E, \mathbf{p})$; $E = \sqrt{\mathbf{p}^2 + m^2}$ for particle mass m ; $f_{Q,\bar{Q}}$ are non-equilibrium distribution functions of quarks and anti-quarks, respectively. Splitting $f_{Q,\bar{Q}}$ by equilibrium (Fermi-Dirac or modified) distribution $f_{Q,\bar{Q}}^0$ and a small deviation $\delta f_{Q,\bar{Q}}$ for quark and anti-quark, i.e.

$$f_{Q,\bar{Q}} = f_{Q,\bar{Q}}^0 + \delta f_{Q,\bar{Q}}, \quad (23)$$

one can separate out the ideal and dissipation part of $T^{\mu\nu}$, N^μ and J^μ as,

$$T^{\mu\nu} = T_0^{\mu\nu} + T_D^{\mu\nu}, \quad (24)$$

$$N^\mu = N_0^\mu + N_D^\mu \text{ and} \quad (25)$$

$$J^\mu = J_0^\mu + J_D^\mu. \quad (26)$$

Here, reversible/ideal part of energy momentum tensor is $T_0^{\mu\nu} = -g^{\mu\nu}P + (\epsilon + P)u^\mu u^\nu$, and N_0^μ , J_0^μ are that of quark/baryon charge current and electric charge current respectively. The dissipation parts of two currents are N_D^μ , J_D^μ and for energy-momentum tensor is,

$$T_D^{\mu\nu} = W^\mu u^\nu + W^\nu u^\mu + \pi^{\mu\nu} + \Pi^{\mu\nu}, \quad (27)$$

where, W^μ represents energy flow, $\pi^{\mu\nu}$ and $\Pi^{\mu\nu}$ are shear and bulk viscous stress tensor respectively. All the dissipative candidates $\pi^{\mu\nu}$, $\Pi^{\mu\nu}$, W^μ and N_D^μ are orthogonal to four velocity of fluid element u^μ . They can be extracted from $T^{\mu\nu}$ and N^μ by their respective connections [65]:

$$\begin{aligned} \pi^{\mu\nu} &= \left\{ \frac{1}{2}(\Delta_\sigma^\mu \Delta_\rho^\nu + \Delta_\rho^\mu \Delta_\sigma^\nu) - \frac{1}{3}\Delta^{\mu\nu} \Delta_{\sigma\rho} \right\} T^{\sigma\rho}, \\ \Pi + P &= -\frac{1}{3}\Delta_{\mu\nu} T^{\mu\nu}, \\ q^\mu &= W^\mu - hN_D^\mu = u_\nu T^{\nu\sigma} \Delta_\sigma^\mu - h\Delta_\nu^\mu N^\nu. \end{aligned} \quad (28)$$

Here, projection operator orthogonal to fluid velocity is $\Delta^{\mu\nu} = g^{\mu\nu} - u^\mu u^\nu$, Π and P are respectively bulk and local isotropic pressure. In practice, four-velocity u^μ is chosen in two ways, known as Eckart and Landau frames. In Eckart frame u^μ is parallel to N^μ and so, $N_D^\mu = 0$. Similarly, $W^\mu = 0$ in Landau frame. For a system with no net charge, the four-velocity in the Eckart formalism is not well defined. Hence, in general under this situation one should use the Landau frame.

The transport coefficients η, ζ, κ and σ are basically proportionality constants, which make connection between thermodynamical forces ($\pi^{\mu\nu}$, $\Pi^{\mu\nu}$, q^μ , E^μ) and the corresponding currents ($\mathcal{U}_\eta^{\mu\nu}$, $\mathcal{U}_\zeta^{\mu\nu}$, \mathcal{U}_κ^μ , J_D^μ) as, [28, 54–56, 59, 66–68]

$$\pi^{\mu\nu} = \eta \mathcal{U}_\eta^{\mu\nu},$$

$$\text{with } \mathcal{U}_\eta^{\mu\nu} = \left(D^\mu u^\nu + D^\nu u^\mu - \frac{2}{3}\Delta^{\mu\nu} \partial_\rho u^\rho \right) \quad (29)$$

$$\Pi^{\mu\nu} = \Pi \Delta^{\mu\nu} = \zeta \mathcal{U}_\zeta^{\mu\nu},$$

$$\text{with } \mathcal{U}_\zeta^{\mu\nu} = \Delta^{\mu\nu} \partial_\rho u^\rho \text{ and } \Pi = \zeta \partial_\rho u^\rho \quad (30)$$

$$q^\mu = \kappa \mathcal{U}_\kappa^\mu,$$

$$\text{with } \mathcal{U}_\kappa^\mu = T \Delta^{\mu\nu} \left(\frac{D_\nu T}{T} - \frac{D_\nu P}{hn} \right); \quad (31)$$

$$J_D^\mu = \sigma^{\mu\nu} E_\nu, \text{ with } E^\nu = (0, E^i). \quad (32)$$

Here, $D^\mu = \partial^\mu - u^\mu u^\sigma \partial_\sigma$ and, $E^\mu \equiv F^{0\mu}$ contains electric field part only of electromagnetic field tensor $F^{\mu\nu}$. Using Gibbs-Duhem relation,

$$\frac{D_\nu P}{\rho} = h \frac{D_\nu T}{T} - T D_\nu \left(\frac{\mu}{T} \right), \quad (33)$$

Eq. (31) can be further simplified as

$$\mathcal{U}_\kappa^\mu = \frac{T^2}{h} \Delta^{\mu\nu} D_\nu \left(\frac{\mu}{T} \right). \quad (34)$$

Now, owing to the microscopic relations, given in Eq. (20), Eq. (21) and Eq. (22), and then using Eq. (28), we can get

$$\begin{aligned} \pi^{\mu\nu} &= 2N_f N_c \left[\frac{1}{2}(\Delta_\sigma^\mu \Delta_\rho^\nu + \Delta_\rho^\mu \Delta_\sigma^\nu) \right. \\ &\quad \left. - \frac{1}{3}\Delta^{\mu\nu} \Delta_{\sigma\rho} \right] \int \frac{d^3\mathbf{p}}{(2\pi)^3} \frac{p^\sigma p^\rho}{E} (\delta f_Q + \delta f_{\bar{Q}}) \end{aligned} \quad (35)$$

$$\Pi = 2N_f N_c \left[-\frac{1}{3} \Delta_{\mu\nu} \right] \int \frac{d^3 \mathbf{p}}{(2\pi)^3} \frac{p^\mu p^\nu}{E} (\delta f_Q + \delta f_{\bar{Q}}) \quad (36)$$

$$q^\mu = 2N_f N_c \int \frac{d^3 \mathbf{p}}{(2\pi)^3} \Delta_\sigma^\mu \left[\left\{ u_\nu \frac{p^\nu p^\sigma}{E} - h \frac{p^\sigma}{E} \right\} \delta f_Q + \left\{ u_\nu \frac{p^\nu p^\sigma}{E} + h \frac{p^\sigma}{E} \right\} \delta f_{\bar{Q}} \right] \quad (37)$$

$$\text{and } J_D^\mu = 2N_c \sum_{Q=u,d} \int \frac{d^3 \mathbf{p}}{(2\pi)^3} \frac{p^\mu}{E} (e_Q \delta f_Q + e_{\bar{Q}} \delta f_{\bar{Q}}) \quad (38)$$

In local rest frame, four velocity $u = (1, \mathbf{0})$, $p \cdot u = E$, and hence, Eq. (37) can be written as

$$q^\mu = 2N_f N_c \int \frac{d^3 \mathbf{p}}{(2\pi)^3} \frac{p^\mu}{E} \left\{ (E - h) \delta f_Q + (E + h) \delta f_{\bar{Q}} \right\}. \quad (39)$$

The small deviation of the (Fermi-Dirac or modified) distribution function can be assumed as

$$\begin{aligned} \delta f_{Q,\bar{Q}} = (f_{Q,\bar{Q}} - f_{Q,\bar{Q}}^0) &\propto -\frac{\partial f_{Q,\bar{Q}}^0}{\partial E} \\ &\propto \beta f_{Q,\bar{Q}}^0 (1 - f_{Q,\bar{Q}}^0) \\ &= \phi^{(Q,\bar{Q})} \beta f_{Q,\bar{Q}}^0 (1 - f_{Q,\bar{Q}}^0), \end{aligned} \quad (40)$$

where $\phi^{(Q,\bar{Q})}$ will contribute to dissipative part of energy-momentum tensor $T_D^{\mu\nu}$, quark/baryon charge current N_D^μ , electric charge current J_D^μ , as defined in Eqs (23)-(26). To satisfy Landau-Lifshitz condition $u^\mu T_D^{\mu\nu} = 0$, a natural choice is to use the same tensorial decomposition, as defined in Eqs. (29)-(32). Hence $\phi^{(Q,\bar{Q})}$ can be expressed as a function of space time and momentum as [28, 54, 56, 66–68]

$$\begin{aligned} \phi^{(Q,\bar{Q})} &= A_{\mu\nu}^{(Q,\bar{Q})} \mathcal{U}_\eta^{\mu\nu} + B_\mu^{(Q,\bar{Q})} \mathcal{U}_\kappa^\mu + C_\mu^{(Q,\bar{Q})} E^\mu \\ &\quad + Z^{(Q,\bar{Q})} (\partial_\rho u^\rho). \end{aligned} \quad (41)$$

The coefficient factors $A_{\mu\nu}$, B_μ , C_μ and Z for different thermodynamical tensors $\mathcal{U}_\eta^{\mu\nu}$, \mathcal{U}_κ^μ , E^μ and $(\partial_\rho u^\rho)$ are associated with corresponding transport coefficients η , κ , σ and ζ respectively. These coefficient factors can be obtained with the help of Boltzmann equation,

$$\begin{aligned} \frac{\partial f_{Q,\bar{Q}}}{\partial t} + \frac{\partial x^i}{\partial t} \frac{\partial f_{Q,\bar{Q}}}{\partial x^i} + \frac{\partial p^i}{\partial t} \frac{\partial f_{Q,\bar{Q}}}{\partial p^i} &= \left(\frac{\partial f_{Q,\bar{Q}}}{\partial t} \right)_{\text{col}} \\ \Rightarrow \frac{\partial f_{Q,\bar{Q}}}{\partial t} + v^i \frac{\partial f_{Q,\bar{Q}}}{\partial x^i} + F^i \frac{\partial f_{Q,\bar{Q}}}{\partial p^i} &= \left(\frac{\partial f_{Q,\bar{Q}}}{\partial t} \right)_{\text{col}}, \end{aligned} \quad (42)$$

where v^i is particle velocity, F^i is applied force on the particle. The right hand side of Eq. (42), representing

the collisional term (accounting for the forces acting between particles in collisions), can be approximated by Anderson-Witting collision term [53],

$$\left(\frac{\partial f_{Q,\bar{Q}}}{\partial t} \right)_{\text{col}} = - \left(\frac{p^\mu u_\mu}{E} \right) \frac{\delta f_{Q,\bar{Q}}}{\tau_{Q,\bar{Q}}}. \quad (43)$$

This is standard relaxation time approximation (RTA) technique, where $\tau_{Q,\bar{Q}}$ is the rough time scale required for the particle/anti-particle to relax from its non-equilibrium distribution $f_{Q,\bar{Q}}$ to equilibrium distribution $f_{Q,\bar{Q}}^0$. Using Eq. (43) in Eq. (42) and then express that RTA based Boltzmann transport equation in covariant form as

$$\frac{1}{E} p^\mu \partial_\mu f_{Q,\bar{Q}} + e_{Q,\bar{Q}} F^{\mu\nu} \frac{p_\nu}{E} \frac{\partial f_{Q,\bar{Q}}}{\partial p^\mu} = - \left(\frac{p^\mu u_\mu}{E} \right) \frac{\delta f_{Q,\bar{Q}}}{\tau_{Q,\bar{Q}}}. \quad (44)$$

In right hand side (rhs), $\delta f_{Q,\bar{Q}}$ can be expressed in terms of corresponding tensors ($\mathcal{U}_\eta^{\mu\nu}$, $(\partial_\rho u^\rho)$, \mathcal{U}_κ^μ and $E^\mu \equiv F^{0\mu}$), associated with the transport coefficients (η , ζ , κ and σ), by using the Eq. (41). In left hand side (lhs), we will assume $f_{Q,\bar{Q}} \approx f_{Q,\bar{Q}}^0$. Let us proceed for FD distribution of NJL model but the same steps can be done for modified distribution of PNJL/EPNJL model if we follow the Appendix, given in Sec. (VIB). We can write FD distribution in covariant form:

$$f_{Q,\bar{Q}}^0 = 1 / \{ \exp \left(\frac{p^\mu u_\mu \mp \mu}{T} \right) + 1 \}, \quad (45)$$

where p^μ is particle quantity (four momentum) and u^μ , T , μ are fluid quantities, which depend on space and time. So Eq. (44) will get the modified form:

$$\begin{aligned} \frac{1}{E} p^\mu \partial_\mu f_{Q,\bar{Q}}^0 + e_{Q,\bar{Q}} F^{\mu\nu} \frac{p_\nu}{E} \frac{\partial f_{Q,\bar{Q}}^0}{\partial p^\mu} &= - \left(\frac{p^\mu u_\mu}{ET} \right) \frac{1}{\tau_{Q,\bar{Q}}} \\ &\quad \left[A_{\mu\nu}^{(Q,\bar{Q})} \mathcal{U}_\eta^{\mu\nu} + B_\mu^{(Q,\bar{Q})} \mathcal{U}_\kappa^\mu + C_\mu^{(Q,\bar{Q})} E^\mu \right. \\ &\quad \left. + Z^{(Q,\bar{Q})} (\partial_\rho u^\rho) \right] f_{Q,\bar{Q}}^0 (1 - f_{Q,\bar{Q}}^0). \end{aligned} \quad (46)$$

Now, the idea is to express the lhs of Eq. (46) in terms of the tensors, sitting in rhs, so that we can equate their coefficients in both side and get the expressions of $A^{\mu\nu}$, B^μ , C^μ and Z . The first term of lhs in Eq. (46) can be expressed in terms of $\mathcal{U}_\eta^{\mu\nu}$, \mathcal{U}_κ^μ and $\partial_\rho u^\rho$ [28, 54, 56], whereas second term of lhs in Eq. (46) can be expressed in terms of $E^\mu \equiv F^{0\mu}$ [66–68], and then one can find,

$$\begin{aligned} A_{\mu\nu}^{(Q,\bar{Q})} &= \tau_{Q,\bar{Q}} \frac{p_\mu p_\nu}{E}, \\ B_\mu^{(Q,\bar{Q})} &= \tau_{Q,\bar{Q}} \frac{\beta p_\mu}{E} (E \mp h), \\ C_\mu^{(Q,\bar{Q})} &= \tau_{Q,\bar{Q}} \frac{e_{Q,\bar{Q}} p_\mu}{E} \\ \text{and, } Z^{(Q,\bar{Q})} &= \tau_{Q,\bar{Q}} \frac{1}{3E} \left[\mathbf{p}^2 - 3c_s^2 \left(E^2 - T^2 \frac{dM_Q^2}{dT^2} \right) \right], \end{aligned} \quad (47)$$

where bulk viscosity component $Z^{(Q,\bar{Q})}$ is obtained for $\mu = 0$, but components of shear viscosity ($A_{\mu\nu}^{(Q,\bar{Q})}$) and electrical conductivity ($C_\mu^{(Q,\bar{Q})}$) can be used for both $\mu = 0$ and $\mu \neq 0$ (just by changing distribution function). The component of thermal conductivity $B_\mu^{(Q,\bar{Q})}$ is relevant for

$\mu \neq 0$ as it carries the quantity - enthalpy per particle h , which is diverged at $\mu = 0$. The detail calculation of above outcome is given in Appendix (VIA).

Now, using Eqs. (47) in Eq. (41), Eq. (40) and then in Eqs.(35, 36, 38, 39), we get

$$\pi^{\mu\nu} = 2N_F N_c \left\{ \frac{1}{2} (\Delta_\sigma^\mu \Delta_\rho^\nu + \Delta_\rho^\mu \Delta_\sigma^\nu) - \frac{1}{3} \Delta_{\sigma\rho}^{\mu\nu} \right\} \int \frac{d^3 \mathbf{p}}{(2\pi)^3} \left(\frac{p^\sigma p^\rho}{E} \right) \beta \left(\frac{p^\alpha p^\beta}{E} \right) \left\{ \tau_Q f_Q^0 (1 - f_Q^0) + \tau_{\bar{Q}} f_{\bar{Q}}^0 (1 - f_{\bar{Q}}^0) \right\} \mathcal{U}_{\alpha\beta}^\eta, \quad (48)$$

$$\Pi = 2N_F N_c \int \frac{d^3 \mathbf{p}}{(2\pi)^3} \frac{\beta}{9E^2} \left[\mathbf{p}^2 - 3c_s^2 \left(E^2 - T^2 \frac{dM_Q^2}{dT^2} \right) \right]^2 \left\{ \tau_Q f_Q^0 (1 - f_Q^0) + \tau_{\bar{Q}} f_{\bar{Q}}^0 (1 - f_{\bar{Q}}^0) \right\} (\partial_\rho u^\rho), \quad (49)$$

$$q^\mu = 2N_F N_c \int \frac{d^3 \mathbf{p}}{(2\pi)^3} \left(\frac{p^\mu}{E} \right) \beta^2 \left(\frac{p^\nu}{E} \right) \left\{ \tau_Q (E - h)^2 f_Q^0 (1 - f_Q^0) + \tau_{\bar{Q}} (E + h)^2 f_{\bar{Q}}^0 (1 - f_{\bar{Q}}^0) \right\} \mathcal{U}_\nu^\kappa, \quad (50)$$

$$\text{and } J^\mu = 2N_c \sum_{Q=u,d} \int \frac{d^3 \mathbf{p}}{(2\pi)^3} \left(\frac{p^\mu}{E} \right) \beta \left(\frac{p^\nu}{E} \right) \left\{ e_Q^2 \tau_Q f_Q^0 (1 - f_Q^0) + e_{\bar{Q}}^2 \tau_{\bar{Q}} f_{\bar{Q}}^0 (1 - f_{\bar{Q}}^0) \right\} E_\nu. \quad (51)$$

Now, if we compare Eqs.(48), (49), (50) and (51) with Eqs. (29), (30), (31) and (32), then we can identify the

final expressions of transport coefficients as

$$\eta = \frac{2N_F N_c \beta}{15} \int \frac{d^3 \mathbf{p}}{(2\pi)^3} \left(\frac{\mathbf{p}^2}{E} \right)^2 \left\{ \tau_Q f_Q (1 - f_Q) + \tau_{\bar{Q}} f_{\bar{Q}} (1 - f_{\bar{Q}}) \right\}, \quad (52)$$

$$\zeta = \frac{2N_F N_c \beta}{9} \int \frac{d^3 \mathbf{p}}{(2\pi)^3} \frac{1}{E^2} \left[\mathbf{p}^2 - 3c_s^2 \left(E^2 - M_Q T \frac{dM_Q}{dT} \right) \right]^2 \left\{ \tau_Q f_Q (1 - f_Q) + \tau_{\bar{Q}} f_{\bar{Q}} (1 - f_{\bar{Q}}) \right\}, \quad (53)$$

$$\kappa = \frac{2N_F N_c \beta^2}{3} \int \frac{d^3 \mathbf{p}}{(2\pi)^3} \left(\frac{\mathbf{p}}{E} \right)^2 \left\{ \tau_Q (E - h)^2 f_Q (1 - f_Q) + \tau_{\bar{Q}} (E + h)^2 f_{\bar{Q}} (1 - f_{\bar{Q}}) \right\} \quad (54)$$

$$\text{and, } \sigma = \left(\frac{2N_c \beta}{3} \right) \left(\frac{5e^2}{9} \right) \int \frac{d^3 \mathbf{p}}{(2\pi)^3} \left(\frac{\mathbf{p}}{E} \right)^2 \left\{ \tau_Q f_Q (1 - f_Q) + \tau_{\bar{Q}} f_{\bar{Q}} (1 - f_{\bar{Q}}) \right\}. \quad (55)$$

Here, speed of sound, $c_s^2 = \frac{s}{T(\frac{ds}{dT})_v}$. To simplify the notation, we have put $f_{Q,\bar{Q}}$ in last expressions instead of $f_{Q,\bar{Q}}^0$. We will consider $f_{Q,\bar{Q}}$ as equilibrium distribution function for the last expressions and also all other sections and subsections. FD distribution will be taken as equilibrium distribution for NJL model, while modified distribution, given in Eq. (9), will be considered as equilibrium distribution for PNJL or EPNJL models. This replacement calculation for transport coefficients can be found in Ref. [30]. Here also we have addressed the same in Appendix (VIB).

A. Causal Aspects

Now, above diffusion relations, Eq. (29), (31), (32) don't carry any time information, they are instantaneous relations and therefore violate the causality. Among the huge number of references on it, readers can follow Ref. [60, 61, 63–65, 69, 70] for causal aspects in viscosity, thermal conductivity and electrical conductivity. Here, we will go through causal aspects in shear viscosity estimation only.

To understand acausality problem of Navier-Stokes equation, if we can consider a very small perturbation in energy density $\epsilon \rightarrow \epsilon + \delta\epsilon$ and fluid velocity $u^\mu \rightarrow u^\mu + \delta u^\mu$, then we will get a dispersion relation of diffu-

sion Eq. (29) as [60],

$$\omega = \frac{\eta}{\epsilon + p} k^2, \quad (56)$$

where k is wave vector. Hence, we can get diffusion speed,

$$v_T(k) = \frac{d\omega}{dk} = 2 \frac{\eta}{\epsilon + p} k, \quad (57)$$

which means diffusion speed can be infinite (by crossing speed of light) as k tends to infinite. The Navier-Stokes equation (29) is actually derived from 1st order thermodynamics. But if we consider entropy density up to second order then we can obtain causal hydrodynamics equations [[60–62]] :

$$\pi^{\mu\nu} = \eta(D^\mu u^\nu + D^\nu u^\mu - \frac{2}{3}\Delta^{\mu\nu} D_\alpha u^\alpha + \pi^{\mu\nu} T D(\beta_2/T) - 2\beta_2 D\pi^{\mu\nu} - \beta_2 \pi^{\mu\nu} \partial_\alpha u^\alpha) \quad (58)$$

Which is causal replacement of eq. (29). Realizing the new coefficient β_2 as, $\beta_2 = \frac{\tau_\pi}{2\eta}$ where, τ_π is defined as shear relaxation time, we can get dispersion relation for eq. (58) as [60],

$$\omega - i \frac{\eta}{\epsilon + p} \frac{k^2}{1 + i\omega\tau_\pi} = 0. \quad (59)$$

Then the diffusion speed at very large k becomes:

$$v_T^{max} \equiv \lim_{k \rightarrow \infty} \sqrt{\frac{\eta}{(\epsilon + p)\tau_\pi}}. \quad (60)$$

Here, the subscript T stands for transverse velocity. The diffusion speed will not be greater than the speed of light if

$$\tau_\pi \geq \frac{\eta}{\epsilon + p}, \quad (61)$$

which is observed for all known fluid. One can recover the instantaneous Eq. (29) by using $\tau_\pi = 0$. This fact will be well explored in Sec. (IV B) with different extensions of NJL model.

IV. RESULTS

A. $\mu = 0$ case

In Sec. II, we have discussed about the formalism of different extension components of NJL models like (a) vector interaction (II A), (b) PNJL (II B) and (c) EPNJL (II C). Present article is intended to investigate the comparative role of these different extensions of NJL models on transport coefficients of quark matter, where we will discuss about the results for $\mu = 0$ case in this sub-section. Before that, let us see the thermodynamical quantity like entropy density, which will be required

to measure the fluid property of quark matter. The governing expression is Eq. (18). Fig. (3) shows the T dependence of (normalized) entropy density, where a straight horizontal line (black solid line) denotes its massless value ($s \approx 9.2T^3$), commonly known as Stefan-Boltzmann (SB) limit. Now, the interaction reduces that value as shown by dotted red, dash-dotted blue and dashed green lines in Fig. (3), which are obtained from NJL, EPNJL and PNJL models, respectively. Through these different extended effective QCD models, interaction is mainly mapped through T dependent masses $M(T)$, shown in earlier Fig. (2). Since the thermodynamical phase space part of s is mainly controlled by $M(T)$, so one can mark a similar kind of transition pattern between $M(T)$ and $s(T)$. High T entropy density s of PNJL and EPNJL models are suppressed from SB limits because the FD distributions of NJL model are replaced by their respective modified Polyakov loop distribution. We have also added a curve for constant confinement mass $M = 0.326$ GeV, shown by black solid line, drawn using standard Fermi-Dirac distribution function. It is included to demonstrate that the effective models recover this limiting value at small temperature. Thus all the models (NJL, PNJL and EPNJL) basically reproduce or approach the massive and massless limits at $T \rightarrow 0$ and $T \rightarrow \infty$, respectively.

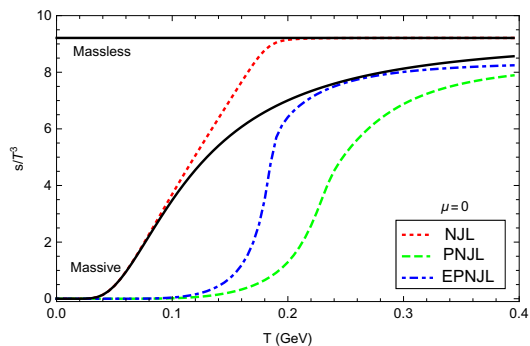


FIG. 3: Normalized entropy density s/T^3 vs temperature T for massive quarks based on NJL (dotted line), EPNJL (dash-dotted line) and PNJL (dashed line) models. As limiting cases we have also shown plots for massless (horizontal solid black line) and massive (black solid line) quarks using standard F-D distribution function. For massive quarks we used confinement mass, which is calculated to be 326 MeV.

Next, we come to the transport coefficients estimations from Eqs. (52), (54), (55) and (53). If we notice the expressions of transport coefficients in Eqs (52), (55), (54), (53) then we can identify two parts, carrying temperature (T) and chemical potential (μ) dependent information. One is relaxation time of medium constituent and another is the thermodynamical part, influenced by its Fermi-Dirac/modified distribution function as well as T , μ dependent mass. At $\mu = 0$, shear viscosity η , bulk viscosity ζ and electrical conductivity σ are relevant transport coefficients, as thermal conductivity κ is diverged/not well-defined at $\mu = 0$. Hence, to zoom in the thermodynamical phase-space part of η , σ and ζ ,

we have plotted $\eta/(\tau T^4)$, $\sigma/(\tau T^2)$ and $\zeta/(\tau T^4)$ vs T in Fig. 4(a), (b) and (c) respectively. Interestingly, we can

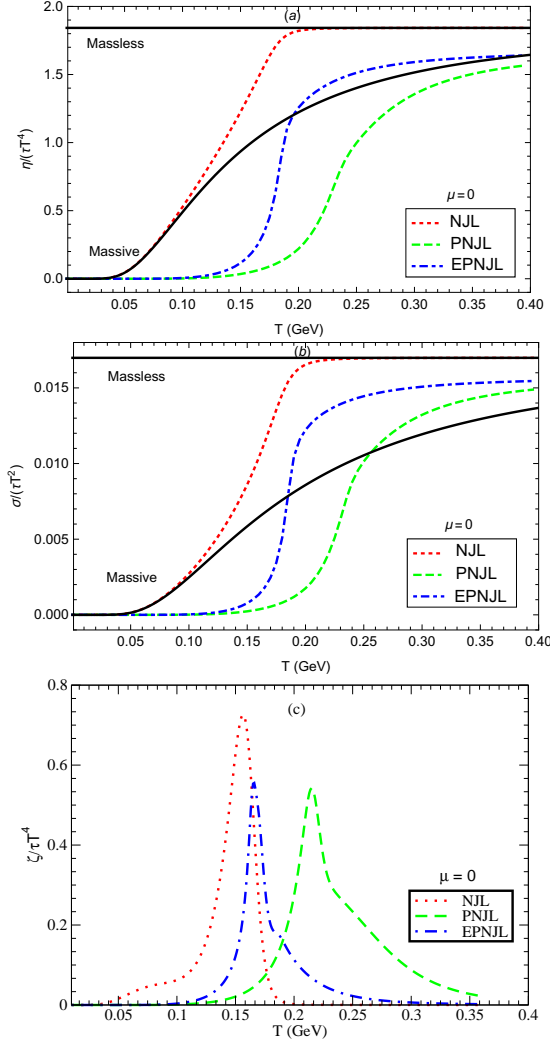


FIG. 4: Normalized (a) shear viscosity $\eta/(\tau T^4)$, (b) electrical conductivity $\sigma/(\tau T^2)$, (c) bulk viscosity $\zeta/(\tau T^4)$ vs temperature T for massive quarks based on NJL (dotted line), EPNJL (dash-dotted line) and PNJL (dashed line) models. As limiting cases we have also shown plots for massless (horizontal solid black line) and massive (black solid line) quarks using standard F-D distribution function. For massive quarks we used confinement mass, which is calculated to be 326 MeV.

find similar kind of pattern in $\eta/(\tau T^4)$, $\sigma/(\tau T^2)$ as we have found for s/T^3 . It is because all are basically mapping approximately similar kind of (normalized) thermodynamical phase-space components. Therefore, according to their rapid changing point in temperature axis, different extended models follow same ranking. NJL melts first at low T , then EPNJL and then PNJL at relatively high T . Bulk viscosity in Fig. 4(c) shows peaks near the transition temperatures of the respective models, as expected [19]. There will be two sources, for which bulk viscosity contribution becomes maximum near transition temperature. First and dominant sources is the interac-

tion measure of thermodynamics $\epsilon - 3P$, which is vanished in massless medium or high temperature QCD medium but become non-zero in the intermediate and low temperature regions. LQCD as well as effective QCD model calculations like NJL exhibit maximum interaction measure near transition temperature. Being proportional with interaction measure ($\zeta \propto (\epsilon - 3P)$), bulk viscosity displays similar kind of peak structure near transition temperature. This interaction measure can alternatively be understood as $(\frac{1}{3} - c_s^2)$, which basically interprets the deviation of speed of sound square from its massless value $1/3$. This $\zeta \propto (\frac{1}{3} - c_s^2) \propto (\epsilon - 3P)$ relation is thus main source for exhibiting the peak pattern of bulk viscosity, which alternatively reveals the conformal breaking structure of QCD medium [19]. Another source is the quantity $\frac{dM}{dT}$, which shows peak structure near chiral transition temperature T_Σ . Sitting in the expression of bulk viscosity, $\frac{dM}{dT}$ and $(\frac{1}{3} - c_s^2)$ become two sources to amplify the peak structure.

TABLE I: Locations of temperatures (MeV), where different temperature dependent quantities - quark condensate Σ , Polyakov loop Φ , s/T^3 , $\eta/(\tau T^4)$, $\sigma/(\tau T^2)$ show their change/transition (for $\mu = 0$ case).

Models	Σ	Φ	s/T^3	$\eta/(\tau T^4)$	$\sigma/(\tau T^2)$
NJL	177	-	two peak	165	172
PNJL	233	228	230	230	232
EPNJL	185	183	184	183	185

At the end of Sec. (IIC), we have discussed about quark condensate Σ [73] and Polyakov loop Φ , which change with T to map the chiral and confinement-deconfinement phase transitions, respectively. The order parameter (Σ) can be estimated from NJL model, while PNJL and EPNJL can describe both order parameters (Σ , Φ). The transition temperatures T_Σ and T_Φ are basically the inflection points, which are calculated by taking the derivative of the corresponding order parameter with respect to T and then finding the extremum for that. The quantities s/T^3 , $\eta/(\tau T^4)$ and $\sigma/(\tau T^2)$ are quite interesting as they contain collective effect of both the order parameters. Table (I) documents the values of these temperatures for order parameters - quark condensate Σ , Polyakov loop Φ and as well as for the quantities s/T^3 , $\eta/(\tau T^4)$ and $\sigma/(\tau T^2)$. The temperatures for the transport coefficients and the entropy density have been estimated in the same fashion as it is done for the order parameters. From the expressions of s/T^3 , $\eta/(\tau T^4)$ and $\sigma/(\tau T^2)$, written above, one notices that $\Sigma(T)$ enters through $M(T)$, while $\Phi(T)$ enters through both $M(T)$ and thermal distribution functions. Though two order parameters enter in the expressions of s/T^3 , $\eta/(\tau T^4)$ and $\sigma/(\tau T^2)$ in the same ways, but their momentum dependent integrands are different and therefore, they are not showing the same temperatures, as evident from table (I). The differences are more evident for NJL model; as one

introduces the background gauge field in PNJL or EPNJL model the differences almost vanish and the temperatures calculated from these quantities are almost similar to those calculated from the order parameters. Only s/T^3 in NJL model exhibit two peak structure instead of one peak, which is a model-parameter dependent fact. So, ignoring this fact we can roughly conclude that the transition points of s/T^3 , $\eta/(\tau T^4)$ and $\sigma/(\tau T^2)$ are close to average values of T_Σ and T_Φ for PNJL and EPNJL models.

B. Perfect fluid and Causal aspects

We have normalized information of τ during plotting shear viscosity in Fig. (4), but it can also be a temperature dependent quantity, if one attempts to calculate it microscopically and $\tau(T)$ can modify the T dependent profile of shear viscosity as well as other transport coefficients. From experimental side, η/s of quark matter created at RHIC is found to be very close to its lower bound $\frac{1}{4\pi}$, based on viscous hydrodynamic model analysis of elliptic flow [13]. We may get a rough idea about the values of τ , for which our estimated η/s will be close to the lower bound. This restriction also give us a temperature dependent τ instead of its constant value. For massless spin 1/2 particle with zero chemical potential, $\tau = 5/4\pi T$ give us $\eta/s = 1/4\pi$. This is shown as the black line in the Fig. 5. Imposing same restriction of $\eta/s = 1/4\pi$ in NJL, PNJL and EPNJL model calculations, we get required relaxation time $\tau(T)$, displayed by dotted, dashed and dash-dotted lines in Fig. (5). Let us analyze these curves. We know that (approximately) massless quark can only be expected at very high temperature but as we decrease the temperature, the non-zero quark condensate will form, for which constituent quark mass also grows up. Mapping this fact via gap equation in NJL model, thermodynamical part of η become suppressed in low temperature domain with respect to the massless case. This lower value of thermodynamical part can be compensated by little higher values of τ for getting same values of $\eta/s (= 1/4\pi)$ as obtained in massless case. Therefore red dotted line (τ of NJL model) is quite larger than black solid line (τ of massless case) in low temperature domain. Above the transition temperature, both curves are merged as condensate melts down completely. When we transit to PNJL model, the confinement picture has been taken into consideration (statistically) via modified thermal distribution function, which has lower statistical weight than FD distribution. So, with respect to NJL case, PNJL has lower strength for thermodynamical part of η , so for getting KSS[74] limits of η/s , it needs little larger values of τ , shown by green dash line in Fig. (5). The EPNJL curve sits in between NJL and PNJL curves as expected from their $M(T)$ pattern in Fig. (2).

In Sec. (IV B), we have discussed about the causal aspects of dissipation phenomena. Dissipation current and

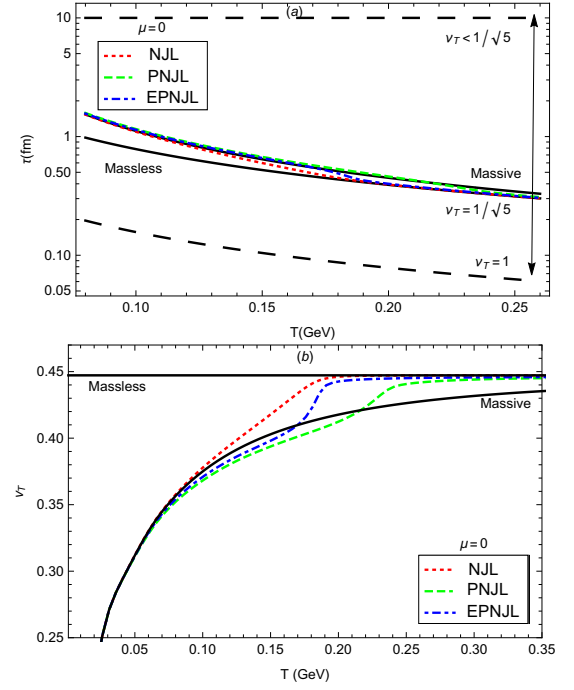


FIG. 5: (a) Temperature dependence of relaxation time in NJL, PNJL and EPNJL models, for which we get $\eta/s = 1/4\pi$. For comparison we have also given plots for massless and massive (with confinement mass, 326 MeV) quarks, using standard F-D statistics. (b) Corresponding maximum values of diffusion speed v_T .

forces are linked instantaneously by Eqs. (29), (31), (32), which means they are communicated via infinite diffusion velocity ($v_T \rightarrow \infty$) and hence, causally disconnected. Through the Eq. (58), the causal connection between shear-channel force and current can be established by introducing finite shear relaxation time τ_π . The relaxation time τ , discussed earlier, can be called collisional relaxation time to distinguish it from shear relaxation time τ_π . To zoom in their differences, one can think τ as microscopic time scale, which is originated from microscopic collision, while τ_π can be considered as macroscopic time scale, required to satisfy causality. In practice, we take $\tau_\pi \approx \tau$ but actually they are different time scale, which is pointed out in Ref. [65]. A rigorous relation in RTA [63] can connect them by relation:

$$\begin{aligned} \tau_\pi &= \tau \left(\frac{u^\mu k_\mu}{T} \right)^\lambda \\ &= \tau \left(\frac{E}{T} \right)^\lambda \text{ (in fluid rest frame) ,} \end{aligned} \quad (62)$$

where λ is unknown parameter. So the inequality, given in Eq. (61), will get a rigorous form:

$$\begin{aligned} \tau_\pi &> \frac{\eta}{(\epsilon + P)} \\ \tau \left(\frac{E}{T} \right)^\lambda &> \frac{\beta_\pi \tau}{(\epsilon + P)} \end{aligned}$$

$$\Rightarrow v_T^{max} = \sqrt{\frac{\beta_\pi}{(\epsilon + P)} \left(\frac{T}{E}\right)^\lambda} < 1, \quad (63)$$

where $\eta = \beta_\pi \tau$ is assumed. In general, we consider $\lambda = 0$, which means $\tau_\pi = \tau$, i.e. the inequality becomes

$$v_T^{max} = \sqrt{\frac{\beta_\pi}{(\epsilon + P)}} < 1 \quad (64)$$

The maximum value of diffusion speed, from Eq. (60), can be written for massless case as

$$v_T^{max} \equiv \sqrt{\frac{\tau}{5\tau_\pi}}, \quad (65)$$

since $\eta = \tau(\epsilon + P)/5$ for massless fermionic/bosonic medium. Now, one can easily recognize that $\tau_\pi \rightarrow 0$ in Eq. (60) or (65) give us $v_T^{max} \rightarrow \infty$. Hence to mention relativistic inequality $v_T^{max} \leq 1$, massless matter should follow the inequality:

$$\tau_\pi \geq \frac{\tau}{5}. \quad (66)$$

This lower limit of τ_π ($= \tau/5$) is drawn by long dash line in Fig. 5(a). So in principle, τ_π can be lower or greater than τ but we can bound it within the inequality: $\frac{\tau}{5} \leq \tau_\pi \leq 10$ fm, where upper limit has been fixed from phenomenological side, by assuming 10 fm life time of medium (shown by straight horizontal long dash line). For $\tau_\pi \approx \tau$ approximation, $v_T^{max} = 1/\sqrt{5}$ massless case and $v_T^{max}(T)$ for NJL, PNJL and EPNJL models are drawn in Fig. 5(b), where all curves follow $v_T^{max} \leq 1/\sqrt{5}$, since we assume $\tau_\pi \approx \tau$. However, we should accept that the general form of v_T^{max} (at $\mu = 0$):

$$v_T^{max} = \sqrt{\left(\frac{T}{E}\right)^\lambda \left[\frac{\frac{\beta}{15} \int \frac{d^3\mathbf{p}}{(2\pi)^3} \left(\frac{\mathbf{p}^2}{E}\right)^2 f_Q(1-f_Q)}{\int \frac{d^3\mathbf{p}}{(2\pi)^3} \left(\frac{\mathbf{p}^2}{3E} + E\right) f_Q} \right]}, \quad (67)$$

whose massless limit should be

$$\lim_{m \rightarrow 0} = \sqrt{\left(\frac{1}{3}\right)^\lambda \left[\frac{1}{5}\right]}, \quad (68)$$

where roughly average energy can be considered as $E \approx 3T$. Here, we have generated our numerical values for $\lambda = 0$ i.e. for $\tau_\pi = \tau$ instead of going any general form. At high T , all are merged to massless limit as expected and at low T , the values of $v_T^{max}(T)$ are quite lower. It means that at low T domain, τ_π is quite larger i.e. quite safer zone for causal aspects. The inequality $\frac{\tau}{5} \leq \tau_\pi \leq 10$ fm is shown by arrow in Fig. 5(a), where corresponding approximated values of v_T^{max} are displayed in different zones. Here also, we have put massless ($M = 0$) and confinement mass ($M = 0.300$ GeV) curves (two solid black line) for $\tau_\pi = \tau$ in Fig. 5(a), (b).

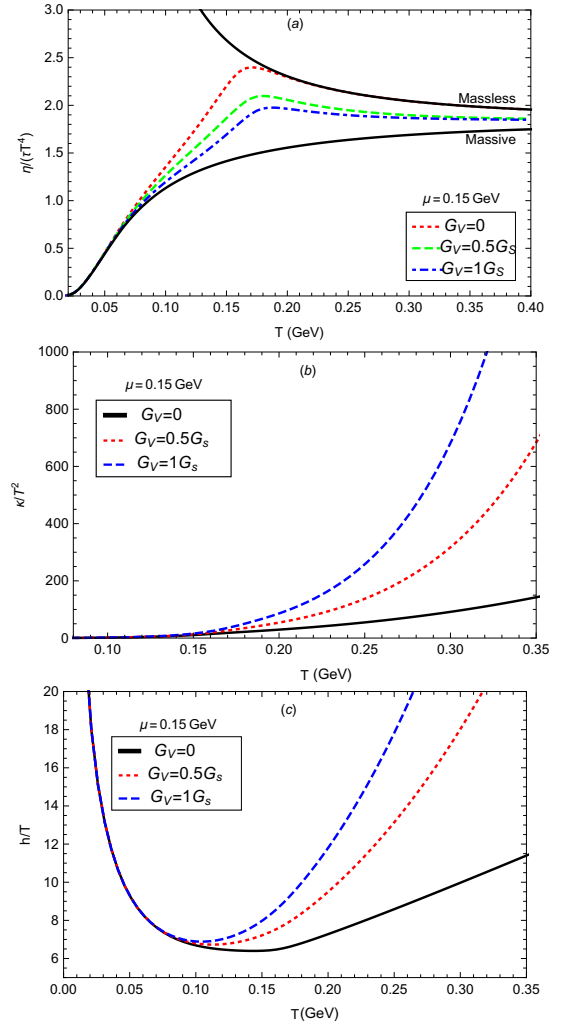


FIG. 6: Finite density plots at different values of G_V for (a) normalized shear viscosity, (b) thermal conductivity and (c) heat function as a function of T , in NJL model.

C. Finite μ Results

Now, let us move to finite μ results, where we can explore the estimation of thermal conductivity κ , which can not be studied in $\mu = 0$ picture. However thermal diffusion coefficients can be estimated at $\mu = 0$ (see in Ref. [65]). We also explore the effect of vector interaction, the incorporation of which becomes almost indispensable at nonzero μ . In Fig. 6(a), we have plotted $\eta/(\tau T^4)$ against T -axis for $\mu = 0.150$ GeV. For massless case, instead of a horizontal line, as obtained in Fig. 4(a), we are getting a decreasing function of temperature, shown by black solid line in Fig. 6(a). To understand the blowing trend in low temperature range, let us see an analytic form of T -dependence for finite μ by taking some rough assumption, described below.

For $\mu = 0$, massless results of Eq. (52) is

$$\frac{\eta}{\tau T^4} = \left(\frac{7}{8}\right) \left(\frac{\pi^4}{90}\right) \left(\frac{4 \times (4N_F N_c)}{5\pi^2}\right) \approx 1.84, \quad (69)$$

which can be approximated as

$$\frac{\eta}{\tau T^4} = \left(\frac{4 \times (4N_F N_c)}{5\pi^2}\right) \approx 1.94, \quad (70)$$

if we take Maxwell-Boltzmann distribution in place of Fermi-Dirac distribution of quark. Now, for $\mu \neq 0$, Eq. (70) can get a simplified form

$$\begin{aligned} \eta &\approx 2N_f N_c \frac{\beta}{15} \int \frac{d^3 \mathbf{p}}{(2\pi)^3} \tau \left(\frac{\mathbf{p}^2}{E}\right)^2 \left[e^{-\beta(E-\mu)} + e^{-\beta(E+\mu)} \right] \\ &= 2N_f N_c \frac{\beta}{15} \int \frac{d^3 \mathbf{p}}{(2\pi)^3} \tau \mathbf{p}^2 e^{-\beta E} \left[e^{\beta \mu} + e^{-\beta \mu} \right] \\ &= 2N_f N_c \frac{4\tau T^4}{5\pi^2} \left[e^{\beta \mu} + e^{-\beta \mu} \right] \\ \Rightarrow \frac{\eta}{\tau T^4} &= 1.94 \times \cosh(\mu/T), \end{aligned} \quad (71)$$

which can explain the blowing up nature of black solid line in Fig. 6(a), when we decrease the temperature. Now if we revisit again Fig. 4(a), then we see that transition from $m = 0$ to non-zero $M(T)$ provide a large suppression at low T domain, which is realized as the effect of non-perturbative QCD interaction. Hence, in $\mu \neq 0$ picture, the transition of $m = 0 \rightarrow M(T)$ makes the blowing up (black solid) curve be transformed to (red dotted) suppressed curve. Due to this turning, we will get a peak-like behaviour around $T = 160$ MeV. Now we know that with the increase of μ , the transition temperature (T_Σ) decreases. Similarly, transition points for transport coefficients like $\eta/(\tau T^4)$, $\sigma/(\tau T^2)$ as well as thermodynamical quantities are also noticed to be shifted towards lower temperature as μ increases.

Now let us come to the vector interaction picture of NJL model. As we introduce the vector interaction the transition temperature gets modified for a given chemical potential – it starts increasing with the strength of G_V , which basically couples to the chemical potential through the relation $\tilde{\mu} = \mu - G_V n$, $\tilde{\mu}$ being the effective chemical potential. It means that if we increase the value of G_V the value of effective chemical potential decreases, thus the transition temperature increases. Similar transition in the peak-like appearance of $\eta/(\tau T^4)$ is observed and it shifts towards higher T as G_V is increased. Apart from transition points, Fig. 6(a) also shows a decreasing profile for increasing G_V . The reason for the reduction of transport coefficient with vector interaction can be realized as follows. We have already seen in Sec. II A and in Fig. (1), the constituent mass M is slightly enhanced with G_V near the transition temperature. On the other hand effective chemical potential $\tilde{\mu}$ decreases with G_V . These increasing M and decreasing $\tilde{\mu}$ make thermodynamical phase space part of η reduce.

Similar to shear viscosity, electrical conductivity following same pattern (not shown) but totally different variation can be found for thermal conductivity, as shown in Fig. 6(b). For thermal conductivity, heat function h , or more precisely enthalpy density per net baryon/quark density plays an important role. Its temperature dependence is shown in Fig. 6(c), where we see that h increases with G_V at high temperature, which dominantly appears in κ . Now, the reason for increasing h with G_V can be understood as follows. Increasing of G_V make $\tilde{\mu}$ decrease and so, ρ decreases. Hence $h \propto 1/\rho$ increases.

V. SUMMARY

Present article has attempted to explore the effect of different extended components of mean field models on transport coefficients calculations and made a comparison among them. First we start with NJL model which can map chiral phase transition of QCD medium. Here, quark condensate melts down near chiral transition temperature, around which normalized transport coefficients and thermodynamical quantity like entropy density also face maximum changes. While, bulk viscosity is showing peak structure near transition temperature like interaction measure of QCD thermodynamics, observed in LQCD and effective QCD model calculations. Hence, they may be roughly considered as alternative quantities for mapping chiral phase transition. Then to mimic QCD further closely we incorporate the deconfinement dynamics, along with the chiral one, by taking into account the background gauge field through PNJL model. Along with the chiral transition temperature, one can separately identify deconfinement temperature, where Polyakov loop face a rapid change. The transport coefficients along with thermodynamical quantities will exhibit quite interesting profile as they contain both chiral and deconfinement dynamics. Hence, they show their signal like maximum change (shear viscosity, electrical conductivity) or maximum value (bulk viscosity) around an intermediate temperature between chiral and deconfinement transition temperature. After PNJL model, we have considered EPNJL model, which incorporate a strong entanglement between the chiral and deconfinement dynamics to enforce the coincidence of chiral and deconfinement transition temperatures within the range provided by the LQCD. Due to this merging of two transitions temperatures, we notice that order parameters (quark condensate, Polyakov loop), normalized-thermodynamical quantities like entropy density, normalized-transport coefficients like shear viscosity, electrical conductivity are showing their maximum change or transition near same temperature. Bulk viscosity will show peak at that temperature. Massless case and NJL model calculations of transport coefficients are coincided at high temperature, but PNJL and EPNJL results still remain suppressed at high temperature due to transformation of Fermi-Dirac to modified distribution

function.

After exploring the thermodynamical phase-space components of transport coefficients, we have tried to estimate relaxation time of quarks from the phenomenological understanding, which expect that shear viscosity to entropy density ratio will be very close to KSS bound. Imposing that phenomenological expectation, required relaxation time from massless case to NJL to EP-NJL to PNJL model become larger at low temperature, but they merge at high temperature. Defining a shear relaxation time to satisfy causal aspect in the fluid, we have shown its possible range for RHIC/LHC matter. In normal practice, (macroscopic) shear relaxation time is considered to be equal with the (microscopic) particle relaxation time, but in reality the former time scale might be larger or smaller than the latter one. It is causality, which dictates that the shear diffusion speed in medium should not exceed the speed of light, for which we get the lower limit of shear relaxation time. On the other hand, medium life time might be consider as upper limit of shear relaxation time. Since shear diffusion speed from massless case to model calculations faces large suppression at low temperature, therefore, we can say that non-perturbative low temperature zone of QCD is causally more safer zone.

At the end, we have studied the finite quark chemical potential zone of quark matter. Similar features of decreasing transition temperature with increasing chemical potential is reflected through the appropriate shift of a peak-like appearance of normalized transport coefficients to a lower value of temperature. Role of vector interaction in NJL model and estimation of thermal conductivity at finite quark chemical potential are also investigated.

Acknowledgment: CAI would like to thank his institute, Tata Institute of Fundamental Research (India)

funded by Department of Atomic Energy (DAE), Govt. of India. He would also like to acknowledge the University of Chinese Academy of Sciences, China for financial support. SG and JD acknowledge IIT Bhilai, funded by Ministry of Human Resource Development (MHRD), Govt. of India. Authors are thankful to Amaresh Jashwal for useful discussion.

VI. APPENDIX

A. LHS of RBE

Here, we will address the detail calculation on left hand side (LHS) of RBE, as given in Eq. (46) and see how it can be converted to different (thermodynamical) gradient tensors, associated with shear viscosity, bulk viscosity, thermal conductivity, electrical conductivity. Reader can find corresponding calculations of shear viscosity, bulk viscosity parts from Refs. [28, 54, 56], thermal conductivity part from Refs. [28, 56] and electrical conductivity part from Refs. [66, 67] separately but here we present in a combined form. The FD distribution function, given in Eq. (45), depends on macroscopic quantities or fluid-element quantities - temperature T , chemical potential μ and four velocity u^μ , which can depend on x in local equilibrium picture. It also depend on microscopic quantity or particle quantity - four momentum p^μ , which will not have any x dependence. So Eq. (45) can be re-written in local equilibrium picture as

$$f_{Q,\bar{Q}}^0 = 1/\{\exp\left(\frac{p^\nu u_\nu(x) \mp \mu(x)}{T(x)}\right) + 1\} . \quad (72)$$

Using Eq. (72) in first term of LHS of Eq. (46), we get

$$\begin{aligned} \frac{p^\mu}{E} \partial_\mu f_{Q,\bar{Q}}^0 &= -\frac{\exp\left(\frac{p^\nu u_\nu(x) \mp \mu(x)}{T(x)}\right)}{\{\exp\left(\frac{p^\nu u_\nu(x) \mp \mu(x)}{T(x)}\right) + 1\}^2} \left[\frac{p^\mu}{E} \partial_\mu \left\{ \frac{p^\nu u_\nu(x) \mp \mu(x)}{T(x)} \right\} \right] \\ &= -f_{Q,\bar{Q}}^0 (1 - f_{Q,\bar{Q}}^0) \left[\frac{p^\mu p^\nu}{ET(x)} \partial_\mu u_\nu(x) - \frac{p^\mu p^\nu u_\nu}{ET^2(x)} \partial_\mu T(x) \mp \frac{p^\mu}{E} \partial_\mu \left(\frac{\mu(x)}{T(x)} \right) \right] , \\ &= -f_{Q,\bar{Q}}^0 (1 - f_{Q,\bar{Q}}^0) \left[\frac{p^\mu p^\nu}{ET} \left\{ \partial_\mu u_\nu(x) - \frac{u_\nu \partial_\mu T(x)}{T} \right\} + \frac{2}{ET} \frac{dM_Q^2}{dT} u^\mu \partial_\mu T \mp \frac{p^\mu}{E} \partial_\mu \left(\frac{\mu(x)}{T(x)} \right) \right] \end{aligned} \quad (73)$$

Our goal will be to express Eq. (73) in terms of thermodynamical tensor $\mathcal{U}_\eta^{\mu\nu}$, $\partial_\rho u^\rho$, $\mathcal{U}_\kappa^{\mu\nu}$, connected with η , ζ , κ . Using the identity [54],

$$\frac{\partial_\mu T}{T} = u^\alpha \partial_\alpha u_\mu - c_s^2 u_\mu \partial_\alpha u^\alpha , \quad (74)$$

with square of speed of sound $c_s^2 = \left(\frac{\partial P}{\partial \epsilon} \right)$, we can get

$$\frac{p^\mu}{E} \partial_\mu f_{Q,\bar{Q}}^0 = -f_{Q,\bar{Q}}^0 (1 - f_{Q,\bar{Q}}^0) \left[\frac{p^\mu p^\nu}{2ET} \left\{ D_\mu u_\nu + D_\nu u_\mu - \frac{2}{3} \Delta_{\mu\nu} \partial_\alpha u^\alpha \right\} - \frac{1}{3ET} \left\{ p^\mu p^\nu (\Delta_{\mu\nu} + 3c_s^2 u_\mu u_\nu) \right\} \right]$$

$$\left. - 3c_s^2 T^2 \frac{dM_Q^2}{dT} \right\} (\partial_\rho u^\rho) \mp \frac{p^\mu}{E} \partial_\mu \left(\frac{\mu(x)}{T(x)} \right) \Bigg]. \quad (75)$$

Using Eq. (75) and (46), we get

$$\begin{aligned} -f_{Q,\bar{Q}}^0(1-f_{Q,\bar{Q}}^0) \left[\frac{p^\mu p^\nu}{2ET} \mathcal{U}_\eta^{\mu\nu} - \frac{1}{3ET} \left\{ p^\mu p^\nu (\Delta_{\mu\nu} + 3c_s^2 u_\mu u_\nu) - 3c_s^2 T^2 \frac{dM_Q^2}{dT} \right\} (\partial_\rho u^\rho) \right] \\ = -\left(\frac{p \cdot u}{ET} \right) \frac{1}{\tau_{Q,\bar{Q}}} \left[A_{\mu\nu}^{(Q,\bar{Q})} \mathcal{U}_\eta^{\mu\nu} + Z^{(Q,\bar{Q})} (\partial_\rho u^\rho) \right] f_{Q,\bar{Q}}^0(1-f_{Q,\bar{Q}}^0). \end{aligned} \quad (76)$$

Now, from the above equation comparing the coefficients of $\mathcal{U}_\eta^{\mu\nu}$ and $\partial_\rho u^\rho$ in both side [54],

$$\Rightarrow A_{\mu\nu}^{(Q,\bar{Q})} = \tau_{Q,\bar{Q}} \frac{p_\mu p_\nu}{2E} \quad (\text{using } p \cdot u = E) \quad (77)$$

$$\begin{aligned} \text{and, } Z^{(Q,\bar{Q})} &= -\frac{\tau_{Q,\bar{Q}}}{3E} \left\{ p^\mu p^\nu (\Delta_{\mu\nu} + 3c_s^2 u_\mu u_\nu) - 3c_s^2 T^2 \frac{dM_Q^2}{dT} \right\} \\ &= \tau_{Q,\bar{Q}} \frac{1}{3E} \left[\mathbf{p}^2 - 3c_s^2 \left(E^2 - T^2 \frac{dM_Q^2}{dT^2} \right) \right] \quad (\text{in local rest frame.}) \end{aligned} \quad (78)$$

The solution (Eq. 78) is not unique [54]. One can make a shift $Z^{(Q,\bar{Q})} \rightarrow Z'^{(Q,\bar{Q})} = Z^{(Q,\bar{Q})} - a - bE$, which can also be true. The unknown constants a, b are associated with particle number and energy conservation respectively. Here we calculate bulk viscosity for zero chemical potential ($\mu = 0$), thus $a = 0$. Now, if we have a particular solution of Eq. (78) as $Z_{\text{par}}^{(Q,\bar{Q})}$ which satisfy Landau-Lifshitz condition (fluid frame is at rest with energy flow) then $Z^{(Q,\bar{Q})} = Z_{\text{par}}^{(Q,\bar{Q})} - bE$. With the help of microscopic definition of thermodynamical quantities such as entropy density (s), heat capacity c_V and Eq. 49 we can find the bulk pressure as

$$\Pi = 2N_F N_c \beta \int \frac{d^3 \mathbf{p}}{(2\pi)^3} \frac{Z_{\text{par}}^{(Q,\bar{Q})}}{3E} \left[\mathbf{p}^2 - 3c_s^2 \left(E^2 - T^2 \frac{dM_Q^2}{dT^2} \right) \right] \left\{ f_Q^0(1-f_Q^0) + f_{\bar{Q}}^0(1-f_{\bar{Q}}^0) \right\} (\partial_\rho u^\rho) \quad (79)$$

and,

$$Z_{\text{par}}^{(Q,\bar{Q})} = \tau_{Q,\bar{Q}} \frac{1}{3E} \left[\mathbf{p}^2 - 3c_s^2 \left(E^2 - T^2 \frac{dM_Q^2}{dT^2} \right) \right]. \quad (80)$$

Here, we can express square of speed of sound at $\mu = 0$ as $c_s^2 = \frac{s}{c_V} = \frac{s}{T \left(\frac{ds}{dT} \right)_V}$.

Now, Eq. (73) also carry \mathcal{U}_κ^μ , related with κ , which can be constructed by combining last two terms of Eq. (73):

$$\begin{aligned} -\frac{p^\mu (p \cdot u) \partial_\mu T(x)}{ET^2} \mp \frac{p^\mu}{E} \partial_\mu \left(\frac{\mu(x)}{T(x)} \right) &= \frac{p^\mu}{E} \left\{ -\frac{(p \cdot u) \partial_\mu T(x)}{T^2} \mp \partial_\mu \left(\frac{\mu(x)}{T(x)} \right) \right\} \\ &\equiv \frac{p^i}{E} \left\{ -\frac{E \partial_i T(x)}{T^2} \mp \partial_i \left(\frac{\mu(x)}{T(x)} \right) \right\} \quad (\text{using } p \cdot u = E \text{ and } p^\mu \equiv p^i) \\ &= \frac{p^i}{E} \left\{ \frac{E}{h} \mp 1 \right\} \partial_i \left(\frac{\mu(x)}{T(x)} \right) \quad (\text{Eq. (33) with } \partial_i P = 0 \text{ is } -\frac{\partial_i T}{T^2} = \frac{1}{h} \partial_i (\mu/T)) \end{aligned} \quad (81)$$

Using Eq. (81) in (73) and then in (46), we get

$$\begin{aligned} -f_{Q,\bar{Q}}^0(1-f_{Q,\bar{Q}}^0) \frac{p^i}{E} \left\{ \frac{E}{h} \mp 1 \right\} \partial_i \left(\frac{\mu(x)}{T(x)} \right) + \dots &= -\left(\frac{p \cdot u}{ET} \right) \frac{1}{\tau_{Q,\bar{Q}}} \left[B^i \frac{T^2}{h} \partial_i \left(\frac{\mu(x)}{T(x)} \right) + \dots \right] f_{Q,\bar{Q}}^0(1-f_{Q,\bar{Q}}^0) \\ &\Rightarrow B_{(Q,\bar{Q})}^i = \tau_{Q,\bar{Q}} \frac{p_i}{ET} (E \mp h) \quad (\text{using } p \cdot u = E) \\ &\Rightarrow B_{(Q,\bar{Q})}^\mu = \tau_{Q,\bar{Q}} \frac{p_\mu}{ET} (E \mp h) \end{aligned} \quad (82)$$

On the other hand, the second term of LHS of Eq. (46) can be simplified through 4-vector to 3-vector and again to 4-vector components (i.e. $\mu \rightarrow i \rightarrow \mu$ index) as

$$\begin{aligned}
e_{Q,\bar{Q}} F^{\mu\nu} \frac{p_\nu}{E} \frac{\partial f_{Q,\bar{Q}}^0}{\partial p^\mu} &\equiv e_{Q,\bar{Q}} E^i \frac{\partial f_{Q,\bar{Q}}^0}{\partial p^i} \\
&= -f_{Q,\bar{Q}}^0 (1 - f_{Q,\bar{Q}}^0) \left[e_{Q,\bar{Q}} E^i \frac{\partial}{\partial p^i} \left(\frac{E}{T} \right) \right] \\
&= -f_{Q,\bar{Q}}^0 (1 - f_{Q,\bar{Q}}^0) \left[e_{Q,\bar{Q}} \frac{\vec{E} \cdot \vec{p}}{ET} \right] \\
&= -f_{Q,\bar{Q}}^0 (1 - f_{Q,\bar{Q}}^0) \left[e_{Q,\bar{Q}} \frac{E_\mu p^\mu}{ET} \right].
\end{aligned} \tag{83}$$

Since electromagnetic field tensor $F^{\mu\nu}$ carries only electric fields (as no external magnetic field is considered in the present work), so $F^{\mu\nu} \frac{p_\nu}{E} = F^{0\mu} + F^{ij} \frac{p_j}{E} + \dots = F^{0\mu} = E^\mu$ is used in the above calculations.

Using Eq. (83) in (73) and then in (46), we get

$$\begin{aligned}
-f_{Q,\bar{Q}}^0 (1 - f_{Q,\bar{Q}}^0) \left[e_{Q,\bar{Q}} \frac{E_\mu p^\mu}{ET} \right] + \dots &= -\left(\frac{p \cdot u}{ET} \right) \frac{1}{\tau_{Q,\bar{Q}}} \left[C_\mu^{(Q,\bar{Q})} E^\mu + \dots \right] f_{Q,\bar{Q}}^0 (1 - f_{Q,\bar{Q}}^0) \\
\Rightarrow C^\mu &= \tau_{Q,\bar{Q}} \frac{e_{Q,\bar{Q}} p^\mu}{E}.
\end{aligned} \tag{84}$$

B. PNJL/EPNJL distribution replacement

The modified distribution function, given in Eq. (9), is can be realized as color average of FD distribution of color particle with imaginary chemical potential [30]. Let us write down the FD distribution with imaginary chemical potential Q^i in local equilibrium picture as [71]

$$f_{Q,\bar{Q}}^i = 1 / \{ \exp \left(\frac{p^\nu u_\nu(x) \mp \mu(x) \mp Q^i}{T(x)} \right) + 1 \}, \tag{85}$$

where $Q^i = 2\pi T(+q, 0, -q)$ with dimensionless condensate variable q . The Polyakov loop variable can be expressed as

$$\begin{aligned}
\Phi &= \frac{1}{3} \sum_i e^{i\beta Q_i} \\
&= \frac{1}{3} \{ 1 + 2\cos(2\pi q) \}.
\end{aligned} \tag{86}$$

Let us rename the modified distribution function as f_Φ and rewrite as

$$f_{Q,\bar{Q}}^\Phi = \frac{\Phi e^{-\beta(E \mp \mu)} + 2\bar{\Phi} e^{-2\beta(E \mp \mu)} + e^{-3\beta(E \mp \mu)}}{1 + 3\Phi e^{-\beta(E \mp \mu)} + 3\bar{\Phi} e^{-2\beta(E \mp \mu)} + e^{-3\beta(E \mp \mu)}} = \frac{N}{D} (say) \tag{87}$$

One can easily check the relation between $f_{Q,\bar{Q}}^i$ and $f_{Q,\bar{Q}}^\Phi$ as

$$\begin{aligned}
\frac{1}{3} \sum_i f_{Q,\bar{Q}}^i &= \frac{1}{3} \left[\frac{1}{\exp\{(E \mp \mu \mp i2\pi Tq)/T\} + 1} + \frac{1}{\exp\{(E \mp \mu)/T\} + 1} + \frac{1}{\exp\{(E \mp \mu \pm i2\pi Tq)/T\} + 1} \right] \\
&= \frac{1}{3} \left[\frac{e^{2\beta(E \mp \mu)} \{1 + 2\cos(2\pi q)\} + 2e^{\beta(E \mp \mu)} \{1 + 2\cos(2\pi q)\} + 3}{e^{3\beta(E \mp \mu)} + e^{2\beta(E \mp \mu)} \{1 + 2\cos(2\pi q)\} + e^{\beta(E \mp \mu)} \{1 + 2\cos(2\pi q)\} + 1} \right] \\
&= \left[\frac{e^{2\beta(E \mp \mu)} \Phi + 2e^{\beta(E \mp \mu)} \Phi + 1}{e^{3\beta(E \mp \mu)} + 3e^{2\beta(E \mp \mu)} \Phi + 3e^{\beta(E \mp \mu)} \Phi + 1} \right] \quad (\text{using Eq. (86)}) \\
&= f_{Q,\bar{Q}}^\Phi
\end{aligned} \tag{88}$$

The transport coefficient calculations remain almost same only the terms, associated with distribution will have to be recalculate. When we start our journey from color particle FD distribution $f_{Q,\bar{Q}}^i$, and its color average $\frac{1}{3} \sum f_{Q,\bar{Q}}^i$,

then their derivative with respect to E , p_i and x will have same anatomy as earlier i.e.

$$\begin{aligned}
\frac{1}{3} \sum_i \frac{\partial f_{Q,\bar{Q}}^i}{\partial E} &= -\beta \frac{1}{3} \sum_i f_{Q,\bar{Q}}^i (1 - f_{Q,\bar{Q}}^i), \\
\frac{1}{3} \sum_i \frac{\partial f_{Q,\bar{Q}}^i}{\partial p_i} &= -\beta \frac{1}{3} \sum_i \left(\frac{p_i}{E} \right) f_{Q,\bar{Q}}^i (1 - f_{Q,\bar{Q}}^i), \\
\frac{1}{3} \sum_i \partial_\mu f_{Q,\bar{Q}}^i &= -\frac{1}{3} \sum_i f_{Q,\bar{Q}}^i (1 - f_{Q,\bar{Q}}^i) \partial_\mu \left\{ \frac{p^\nu u_\nu(x) \mp \mu(x)}{T(x)} \right\}
\end{aligned} \tag{89}$$

These relations indicate that anatomy of Eqs. (40), (46), (73) remain same. Only FD distribution is replaced by FD distribution of color particles. Now we have to transform FD distribution of color particles $f_{Q,\bar{Q}}^i$ in Eq. (89) into modified distribution function $f_{Q,\bar{Q}}^\Phi$. We can express the terms $f_{Q,\bar{Q}}^i (1 - f_{Q,\bar{Q}}^i)$ as

$$\begin{aligned}
-\frac{1}{3} \sum_i f_{Q,\bar{Q}}^i (1 - f_{Q,\bar{Q}}^i) &= \frac{1}{3\beta} \sum_i \frac{\partial f_{Q,\bar{Q}}^i}{\partial E} \\
&= \frac{1}{\beta} \frac{\partial f_{Q,\bar{Q}}^\Phi}{\partial E} \\
&= \frac{1}{\beta} \frac{\left(D \frac{\partial N}{\partial E} - N \frac{\partial D}{\partial E} \right)}{D^2}
\end{aligned} \tag{90}$$

If we expand the above expression, we can get

$$\begin{aligned}
\frac{\left(D \frac{\partial N}{\partial E} - N \frac{\partial D}{\partial E} \right)}{D^2} &= \frac{N}{D} \left(1 - \frac{N}{D} \right) + \{ 2D(\Phi e^{-2\beta(E \mp \mu)} + e^{-3\beta(E \mp \mu)}) - 2N^2 \} / D^2 \\
&= f_{Q,\bar{Q}}^\Phi (1 - f_{Q,\bar{Q}}^\Phi) + 2e^{-2\beta(E \mp \mu)} [(1 + e^{-2\beta(E \mp \mu)}) \Phi (1 - \Phi) + e^{-\beta(E \mp \mu)} (1 - \Phi^2)] / D^2 \\
&\approx f_{Q,\bar{Q}}^\Phi (1 - f_{Q,\bar{Q}}^\Phi).
\end{aligned} \tag{91}$$

The extra term in Eq. (91) might be ignored with respect to the dominating term $f_{Q,\bar{Q}}^\Phi (1 - f_{Q,\bar{Q}}^\Phi)$. For numerical

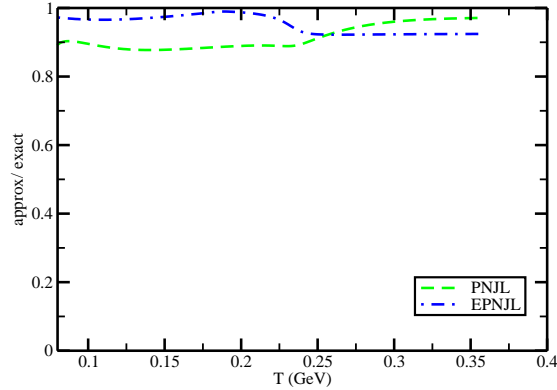


FIG. 7: The ratio between phase-space integration with approximated (excluding extra term) and exact (including extra term) vs T , whose values close to 1 reflects that one may go with this approximation.

check, Fig. (7) has shown the ratio between phase-space integration with approximated (excluding extra term) and exact (including extra term) i.e.

$$\frac{\chi_{\text{approx}}}{\chi_{\text{exact}}} = \frac{\int \frac{d^3 k}{(2\pi)^3} \left[\beta f_0^\Phi (1 - f_0^\Phi) \right]}{\int \frac{d^3 k}{(2\pi)^3} \left[-\frac{1}{3} \sum_i \frac{\partial f_{Q,\bar{Q}}^i}{\partial E} \right]}. \tag{92}$$

We notice that the extra term roughly contribute upto 10%. So one may go safely for rough estimation of different transport coefficients with simplified phase-space factor $\left[\beta f_0^\Phi(1 - f_0^\Phi)\right]$ instead of its complicated version

$\left[-\frac{1}{3}\sum_i \frac{\partial f_{Q,\bar{Q}}^i}{\partial E}\right]$ or $\frac{\left(D\frac{\partial N}{\partial E} - N\frac{\partial D}{\partial E}\right)}{D^2}$. We have shown here susceptibility-type quantity χ , which is basically attached with all transport coefficients, hence this approximation will be valid during estimation transport coefficients or any other quantities, which are proportionally connected with susceptibility. Owing to this assumption, we have used the replacement identity

$$-\frac{1}{3}\sum_i f_{Q,\bar{Q}}^i(1 - f_{Q,\bar{Q}}^i) \approx -f_{Q,\bar{Q}}^\Phi(1 - f_{Q,\bar{Q}}^\Phi) \quad (93)$$

during the calculation of different transport coefficients in PNJL and EPNJL models.

-
- [1] I. A. Shovkovy and P. J. Ellis, *Thermal conductivity of dense quark matter and cooling of stars*, Phys. Rev. C **23** 66 (2002) 015802, hep-ph/0204132.
- [2] C. Manuel, A. Dobado and F. J. Llanes-Estrada, *Shear viscosity in a CFL quark star*, Journal of High Energy Physics 9 (2005) 076, hep-ph/0406058.
- [3] M. G. Alford, H. Nishimura and A. Sedrakian, *Transport coefficients of two-flavor superconducting quark matter*, Phys. Rev. C **90** (2014) 055205, hep-ph/1408.4999.
- [4] S. Sarkar and R. Sharma, *The shear viscosity of two-flavor crystalline color superconducting quark matter*, Phys. Rev. D **96**, 094025 (2017), hep-ph/1701.00010.
- [5] B. Friman, C. Höhne, J. Knoll, S. Leupold, J. Randrup, R. Rapp et al., *The CBM Physics Book: Compressed Baryonic Matter in Laboratory Experiments, Lecture Notes in Physics* (Springer, Berlin Heidelberg, 2011).
- [6] D. Blaschke, J. Aichelin, E. Bratkovskaya, V. Friese, M. Gazdzicki, J. Randrup, O. Rogachevsky, O. Teryaev, and V. Toneev, *Topical issue on exploring strongly interacting matter at high densities—nica white paper*, Eur. Phys. J. A **52**, 267 (2016).
- [7] PHENIX collaboration, S. S. Adler et al., *Elliptic flow of identified hadrons in Au+Au collisions at $s(NN)^{1/2} = 200$ -GeV*, Phys. Rev. Lett. **91** (2003) 182301, nucl-ex/0305013.
- [8] STAR collaboration, J. Adams et al., *Azimuthal anisotropy in Au+Au collisions at $s(NN)^{1/2} = 200$ -GeV*, Phys. Rev. C **72** (2005) 014904, nucl-ex/0409033.
- [9] ALICE collaboration, K. Aamodt et al., *Higher harmonic anisotropic flow measurements of charged particles in Pb-Pb collisions at $\sqrt{sNN}=2.76$ TeV*, Phys. Rev. Lett. **107** (2011) 032301, nucl-ex/1105.3865.
- [10] CMS collaboration, S. Chatrchyan et al., *Multiplicity and transverse momentum dependence of two- and four-particle correlations in pPb and PbPb collisions*, Phys. Lett. B **724** (2013) 213–240, nucl-ex/1305.0609.
- [11] ATLAS collaboration, G. Aad et al., *Measurement of event-plane correlations in $\sqrt{sNN}=2.76$ TeV lead-lead collisions with the ATLAS detector*, Phys. Rev. C **90** (2014) 024905, hep-ex/1403.0489.
- [12] ALICE collaboration, J. Adam et al., *Correlated event-by-event fluctuations of flow harmonics in Pb-Pb collisions at $\sqrt{sNN}=2.76$ TeV*, Phys. Rev. Lett. **117** (2016) 182301, nucl-ex/1604.07663.
- [13] M. J. Tannenbaum, *Recent results in relativistic heavy ion collisions: from ‘a new state of matter’ to ‘the perfect fluid’*, Rep. Prog. Phys. **69** (2006) 2005, nucl-ex/0603003.
- [14] P. Romatschke and U. Romatschke, *Viscosity Information from Relativistic Nuclear Collisions: How Perfect is the Fluid Observed at RHIC?*, Phys. Rev. Lett. **99**, 172301 (2007), nucl-th/0706.1522.
- [15] U. Heinz and R. Snellings, *Collective flow and viscosity in relativistic heavy-ion collisions*, Annu. Rev. Nucl. Part. Sci. **63** (2013) 123, nucl-th/1301.2826.
- [16] P. B. Arnold, G. D. Moore and L. G. Yaffe, *Transport coefficients in high temperature gauge theories. 1. Leading log results*, JHEP 0011 (2000) 001, hep-ph/0010177.
- [17] P. B. Arnold, G. D. Moore and L. G. Yaffe, *Transport coefficients in high temperature gauge theories: (II) Beyond leading log*, JHEP 0305 (2003) 051, hep-ph/0302165.
- [18] J. Ghiglieri, G. D. Moore and D. Teaney, *QCD Shear Viscosity at (almost) NLO*, JHEP 1803, 179 (2018), hep-ph/1802.09535.
- [19] S. Ghosh, T. C. Peixoto, V. Roy, F. E. Serna, G. Krein, *Shear and Bulk Viscosities of Quark Matter from Quark-Meson Fluctuations in the Nambu–Jona-Lasinio model*, Phys. Rev. C **93** (2016) 045205, nucl-th/1507.08798.
- [20] S. Ghosh, F. E. Serna, A. Abhishek, G. Krein, H. Mishra, *Transport responses from rate of decay and scattering processes in the Nambu–Jona-Lasinio model* Phys. Rev. D **99** (2019) 014004, nucl-th/1809.07594.
- [21] S. Ghosh, A. Lahiri, S. Majumder, R. Ray, S. K. Ghosh, *Shear viscosity due to Landau damping from the quark-pion interaction* Phys. Rev. C **88**, 068201 (2013), nucl-th/1311.4070.
- [22] R. Lang and W. Weise, *Shear viscosity from Kubo formalism: NJL model study*, Eur. Phys. J. A **50**, 63 (2014), hep-ph/1311.4628.
- [23] R. Lang, N. Kaiser, and W. Weise, *Shear viscosities from Kubo formalism in a large- N_c Nambu–Jona-Lasinio model* Eur. Phys. J. A **51**, 127 (2015), hep-ph/1506.02459.
- [24] P. Zhuang, J. Hufner, S.P. Klevansky, L. Neise, *Transport properties of a quark plasma and critical scattering at the chiral phase transition* Phys. Rev. D **51**, 3728 (1995).
- [25] P. Rehberg, S.P. Klevansky and J. Hufner, *Elastic Scat-*

- tering and Transport Coefficients for a Quark Plasma in $SU_f(3)$ at Finite Temperatures Nucl. Phys. **A 608**, 356 (1996), hep-ph/9607263.
- [26] C. Sasaki, K. Redlich, *Transport coefficients near chiral phase transition*, Nucl. Phys. **A 832** (2010) 62, hep-ph/0811.4708.
- [27] R. Marty, E. Bratkovskaya, W. Cassing, J. Aichelin, H. Berrehrah, *Transport coefficients from the Nambu–Jona-Lasinio model for $SU(3)_f$* , Phys. Rev. **C 88** (2013) 045204, hep-ph/1311.3159.
- [28] P. Deb, G. Kadam, H. Mishra, *Estimating transport coefficients in hot and dense quark matter*, Phys. Rev. **D 94** (2016) 094002, hep-ph/1603.01952.
- [29] A. Abhishek, H. Mishra, S. Ghosh, *Transport coefficients in the Polyakov quark meson coupling model: A relaxation time approximation*, Phys. Rev. **D 97** (2018) 014005, hep-ph/1709.08013.
- [30] P. Singha, A. Abhishek, G. Kadam, S. Ghosh, H. Mishra, *Calculations of shear, bulk viscosities and electrical conductivity in the Polyakov-quark-meson model* J. Phys. **G 46** (2019) 015201, nucl-th/1705.03084.
- [31] S. K. Ghosh, S. Raha, R. Ray, K. Saha, S. Upadhyaya, *Shear viscosity and phase diagram from Polyakov–Nambu–Jona-Lasinio model*, Phys. Rev. **D 91** (2015) 054005, hep-ph/1411.2765.
- [32] T. Kunihiro, *Quark number susceptibility and fluctuations in the vector channel at high temperatures*, Phys. Lett. **B 271**, 395 (1991),
- [33] S. P. Klevansky, *The Nambu–Jona-Lasinio model of quantum chromodynamics*, Rev. Mod. Phys. **64**, 649 (1992).
- [34] T. Hatsuda and T. Kunihiro, *QCD phenomenology based on a chiral effective Lagrangian*, Phys. Rept. **247**, 221 (1994), hep-ph/9401310.
- [35] M. Buballa, *NJL model analysis of quark matter at large density*, Phys. Rept. **407**, 205 (2005), hep-ph/0402234.
- [36] K. Kashiwa, H. Kouno, T. Sakaguchi, M. Matsuzaki and M. Yahiro, *Chiral phase transition in an extended NJL model with higher-order multi-quark interactions*, Phys. Lett. **B 647**, 446 (2007), nucl-th/0608078.
- [37] S. K. Ghosh, T. K. Mukherjee, M. G. Mustafa and R. Ray, *Susceptibilities and speed of sound from PNJL model*, Phys. Rev. **D 73**, 114007 (2006), hep-ph/0603050.
- [38] S. Mukherjee, M. G. Mustafa and R. Ray, *Thermodynamics of the PNJL model with nonzero baryon and isospin chemical potentials*, Phys. Rev. **D 75**, 094015 (2007), hep-ph/0609249.
- [39] C. Ratti, M. A. Thaler and W. Weise, *Phases of QCD: Lattice thermodynamics and a field theoretical model*, Phys. Rev. **D 73**, 014019 (2006), hep-ph/0506234.
- [40] S. K. Ghosh, T. K. Mukherjee, M. G. Mustafa and R. Ray, *PNJL model with a Van der Monde term*, Phys. Rev. **D 77**, 094024 (2008), hep-ph/0710.2790.
- [41] K. Fukushima, *Phase diagrams in the three-flavor Nambu–Jona-Lasinio model with the Polyakov loop*, Phys. Rev. **D 77**, 114028 (2008), hep-ph/0803.3318.
- [42] S. K. Ghosh, A. Lahiri, S. Majumder, M. G. Mustafa, S. Raha and R. Ray, *Quark Number Susceptibility : Revisited with Fluctuation-Dissipation Theorem in mean field theories*, Phys. Rev. **D 90**, 054030 (2014), hep-ph/1407.7203.
- [43] H. Hansen, W. M. Alberico, A. Beraudo, A. Molinari, M. Nardi and C. Ratti, *Mesonic correlation functions at finite temperature and density in the Nambu–Jona-Lasinio model with a Polyakov loop*, Phys. Rev. **D 75**, 065004 (2007), hep-ph/0609116.
- [44] C. A. Islam, S. Majumder, N. Haque and M. G. Mustafa, *Vector meson spectral function and dilepton production rate in a hot and dense medium within an effective QCD approach*, JHEP **1502**, 011 (2015), hep-ph/1411.6407.
- [45] C. A. Islam, R. Abir, M. G. Mustafa, R. Ray and S. K. Ghosh, *The consequences of $SU(3)$ color singletness, Polyakov Loop and $Z(3)$ symmetry on a quark–gluon gas*, J. Phys. **G 41**, 025001 (2014), hep-ph/1208.3146.
- [46] M. Fukugita and A. Ukawa, *Deconfining and Chiral Transitions of Finite Temperature Quantum Chromodynamics in the Presence of Dynamical Quark Loops*, Phys. Rev. Lett. **57**, 503 (1986),
- [47] Y. Aoki, Z. Fodor, S. D. Katz and K. K. Szabo, *The QCD transition temperature: Results with physical masses in the continuum limit*, Phys. Lett. **B 643**, 46 (2006), hep-lat/0609068.
- [48] Y. Sakai, T. Sasaki, H. Kouno and M. Yahiro, *Entanglement between deconfinement transition and chiral symmetry restoration*, Phys. Rev. **D 82**, 076003 (2010), hep-ph/1006.3648.
- [49] J. Sugano, J. Takahashi, M. Ishii, H. Kouno and M. Yahiro, *Determination of the strength of the vector-type four-quark interaction in the entanglement Polyakov-loop extended Nambu–Jona-Lasinio model*, Phys. Rev. **D 90**, 037901 (2014), hep-ph/1405.0103.
- [50] C. A. Islam, S. Majumder and M. G. Mustafa, *Vector meson spectral function and dilepton rate in the presence of strong entanglement effect between the chiral and the Polyakov loop dynamics*, Phys. Rev. **D 92**, no. 9, 096002 (2015), hep-ph/1508.04061.
- [51] F. Karsch, *Lattice QCD at high temperature and density*, Lect. Notes Phys. **583**, 209 (2002), hep-lat/0106019.
- [52] F. Karsch, E. Laermann and A. Peikert, *Quark mass and flavor dependence of the QCD phase transition*, Nucl. Phys. **B 605**, 579 (2001), hep-lat/0012023.
- [53] L.J. Anderson and H.R. Witting, *A relativistic relaxation-time model for the Boltzmann equation*, Physica **74** (1974) 466-488
- [54] P. Chakraborty and J. I. Kapusta, *Quasi-Particle Theory of Shear and Bulk Viscosities of Hadronic Matter*, Phys. Rev. **C 83**, 014906 (2011), nucl-th/1006.0257.
- [55] A. Hosoya and K. Kajantie, *Transport Coefficients of QCD Matter*, Nucl. Phys. **B 250**, 666 (1985).
- [56] S. Gavin, *Transport Coefficients In Ultrarelativistic Heavy Ion Collisions*, Nucl. Phys. **A 435**, 826 (1985).
- [57] S. Ghosh, *A real-time thermal field theoretical analysis of Kubo-type shear viscosity: Numerical understanding with simple examples*, Int. J. Mod. Phys. **A 29**, 1450054 (2014), nucl-th/1404.4788.
- [58] S. Ghosh, *Electrical conductivity of hadronic matter from different possible mesonic and baryonic loops*, Phys. Rev. **D 95**, no. 3, 036018 (2017), nucl-th/1607.01340.
- [59] D. Fernandez-Fraile and A. Gomez Nicola, *Transport coefficients and resonances for a meson gas in Chiral Perturbation Theory*, Eur. Phys. J. **C 62**, 37 (2009), hep-ph/0902.4829.
- [60] Paul Romatschke, *New Developments in Relativistic Viscous Hydrodynamics*, Int. J. Mod. Phys. **E 19**, no.01, 1-53(2010)
- [61] W. Israel, J.M. Stewart, *Transient relativistic thermodynamics and kinetic theory*, Annals of Physics **118**, 2, (1979), 341-372
- [62] William A. Hiscock and Lee Lindblom, *Stability and*

- causality in dissipative relativistic fluids**, Annals of Physics 151, 466-496 (1983)
- [63] G. S. Denicol, S. Jeon, and C. Gale, *Impact of different extended components of mean field models on transport coefficients of quark matter and their causal aspects* Phys. Rev. C **90**, 024912 (2014).
 - [64] L.P. Csernai, J.I. Kapusta, L. D. McLerran, *Strongly Interacting Low-Viscosity Matter Created in Relativistic Nuclear Collisions* Phys. Rev. Lett. **97** (2006) 152303, nucl-th/0604032.
 - [65] A. Muronga, *Causal theories of dissipative relativistic fluid dynamics for nuclear collisions* Phys. Rev. C **69**, 034903 (2004).
 - [66] A. Puglisi, S. Plumari, V. Greco, *Electric conductivity from the solution of the relativistic Boltzmann equation* Phys. Rev. D **90**, 114009 (2014).
 - [67] G. P. Kadam, H. Mishra, L. Thakur, *Electrical and thermal conductivities of hot and dense hadronic matter* Phys. Rev. D **98** (2018) 114001.
 - [68] M. Greif, I. Bouras, C. Greiner, and Z. Xu, *Electric conductivity of the quark-gluon plasma investigated using a perturbative QCD based parton cascade*, Phys. Rev. D **90**, 094014 (2014).
 - [69] A. Jaiswal, B. Friman, K. Redlich, *Relativistic second-order dissipative hydrodynamics at finite chemical potential* Phys. Lett. B **751**, 548 (2015)
 - [70] J. I. Kapusta, C. Plumberg, *Causal Electric Charge Diffusion and Balance Functions in Relativistic Heavy Ion Collisions* Phys. Rev. C **97**, 014906 (2018).
 - [71] Y. Hidaka, S. Lin, R. D. Pisarski and D. Satow, *Dilepton and photon production in the presence of a nontrivial Polyakov loop* J. High Energy Phys. **10** (2015) 005.
 - [72] *These inflection points can be found by plotting the first temperature-derivative of Σ or Φ as a function of temperature and finding the maximum of the corresponding plot, which signifies the transition temperature T_Σ or T_Φ , respectively. In other words, these are the points at which the curvature changes sign. The readers might look into the Refs. [39, 40, 50] for a detailed discussion, particularly Ref. [50] which involves the same parameter set as used in the present calculation.*
 - [73] not to confused with electrical conductivity
 - [74] KSS (named after the scientists who discovered it, Kovtun-Son-Starinets) is a lower bound on the fluidity of the medium which is the ratio of shear viscosity to entropy density and is found to be equals to $1/4\pi$.